國立臺灣大學電機資訊學院電機工程學研究所

碩士論文

Department of Electrical Engineering

College of Electrical Engineering and Computer Science

National Taiwan University

Master Thesis

複合加減法 3D 列印流程對於多異種的物件製作

Hybrid Additive and Subtractive 3D Printing Process for

Multi-Heterogeneous Objects Fabrication

曾柏凱

Po Kai Tseng

指導教授：羅仁權 博士

Advisor: Ren C. Luo, Ph.D.

中華民國 106 年 7 月

July 2017

誌謝

　　碩士班這兩年是人生中的另一個階段，在這階段中自我充實而且留下一段美好的回憶。兩年的碩士生涯中說長不長說短不短，但是轉眼間來到鳳凰花開的季節，意味我們又將即將往下一個階段邁進。回想起剛來到一個陌生的台大校園，接觸陌生的人事物，一開始還有點憂心與擔心，但進入一個有熱心的學長姊、親切的同學與學弟妹的實驗室，很快就融入生活中。感謝父母，在我面臨低潮時給於我鼓勵與支持，感謝口試委員，張帆人老師以及顏炳郎老師百忙之中特地抽空給予我的論文諸多的建議及指教，感謝指導教授羅仁權教授，不僅提供們豐富的研究資源外，在學術知識上教導我們向深度與廣度發展，在實務方面培養我們動手做的能力，此外，老師還給予我們非常多的國際觀世界觀，並教誨我們待人處事的道理與社會上應對的準則，讓我獲益良多。最後，還要感謝鐿文與東榕學長，與學長討論研究方法和技術瓶頸問題，並一一克服眼前的困難，並且在不斷的摸索中漸漸了解自己的研究興趣，並在未來會繼續朝向此方面更加努力。

　　在國立台灣大學智慧機器人及自動化國際研究中心 (NTU-iCeiRA) 的兩年研究生活中，我要感謝鐿文、瑋隆、獻章、陞祐、繼棠、金成、玲盈、昕昳、東榕、旭佳、禮聰、志遠以及正倫等博班學長姊，還有柏任、士紘、智賢等碩班學長姊，以及同屆共同奮鬥的夥伴達方、俊豪、長鈞、晴岡、李晟、孟勳、靖霖、昱佑、仲凱、莉彤、凱鈞、立揚，最後還有積極認真的學弟妹錦賢、名彥、育榕、石崴、育澤、智堅、武昱、威辰、展嘉、王昊、培淳、嵩詠、何鑫以及曾旻，以及助理雯雅 (Tracy)、煜倫(Dornin)。感謝大家的支持與幫助，不分晝夜地討論研究，同甘共苦地參加比賽熬夜為比賽而努力，在研究之餘還會一起運動一起玩樂，非常開心這段日子能和大家一起奮鬥與生活點滴，你們都是我一生難忘的回憶。

　　能完成這篇論文，我要感謝在我生命中出現的每一個人，真的能遇見你們真好，非常謝謝你們。

<div style="text-align: right">

曾柏凱 謹誌

一百零六年七月

</div>

I

中文摘要

近年來 3D 列印技術越來越流行,並且運用於各種產業,如航太業、工業甚至醫學工程方面,其主要優點為客製化及快速製作,以達到縮短產品週期並提高產品設計之自由度。但是隨著產品的多樣性與複雜性,單純的加工以無法獨力製作完成,因此我們設計出複合加工機(加法及減法),用以完成多樣且複雜的產品。並且產品可能是由多個零件或多個物件所構成的,但目前所使用的 3D 列印都是多個物件同一層先印完再移動至下一層,噴頭會在物件間頻繁移動,不但消耗能源而且拖累完成的時間,因此,在此論文中,我們將提出加法製作多物件流程優化之演算法以及減法路徑規劃完成客製化雕刻。

首先,在加法製作流程優化分為三大步驟,1.針對每個物件作放置之最佳化,以減少列印時所產生支架達到節省材料與去除支架的程序,2.多物件進行集裝優化(bin packing)規劃物件擺放位置,並且結合最短路徑演算法(travelling salesman problem),有利於噴嘴移動過程中,可以使噴嘴有效率之移動,3.加法路徑優化配合硬體上的最大限制,使得列印更加有效率,對比常見方法在演算法中大量減少在物件間移動的頻率,不僅可以節省製作時間外,還可以節約能源。在加減法製作流程,當列印加工完成後並將物件資訊轉換至減法坐標系,並將物件所要雕刻區域利用保角映射(conform mapping)作攤平展開得到二維平面,並使用彈簧質量模型(spring mass model)基於三角形邊長做優化以減小攤平曲面之誤差,接下來二維圖形投影至攤平的二維平面上,再將平面轉換至物件表面,以取得減法路徑軌跡,以完成加減復合之工程,並實現在我們實驗自行開發的龍門式複合加工機上。
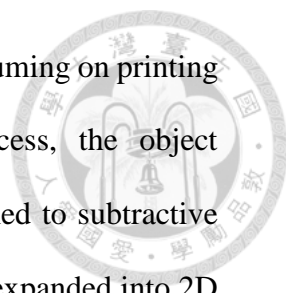
關鍵字:3D 列印技術、複合加工機、集裝優化、最短路徑演算法、龍門式複合加工機

Abstract

In recent years, three dimensional (3D) printing is the fastest growing technology. Nowadays, it has been largely applied in aerospace industry, industry and medicine engineering, etc. Additive manufacturing (AM) technologies not only reduce the new product development cycle, but also develop unique style models to satisfy users' requirements. However, the additive manufacturing cannot complete the diversity and complexity products independently. We design the hybrid 3D printing machine including the additive and subtractive processes to complete the products. And the products may be composed of the many parts or objects. In the common slicing software, the 3D printers print an object layer by layer. However, when multiple objects are printed at the same time, the nozzle moves among objects and always increases enormous distance of the transition travel. Therefore, in this thesis, we propose a novel addition process optimization algorithm and develop the trajectory planning of the subtractive process to carve the customized logo or image.

In the beginning, the optimization of the addition process is divided into three main steps. 1. The optimization for locating each specific object is implemented to minimize the supports during the printing procedure. This step can efficiently save the materials and consume less time for remove the supports. 2. Two dimensional packing problem for planning location of multiple objects is combined with the traveling salesman problem to promote the spray efficiency of nozzle. 3. With consideration of the workspace and hardware limitation, the printing time is apparently decreased by addition path optimization. Compared with the common path planning strategy, the advantage of the proposed path planning minimizes the frequency of movement among
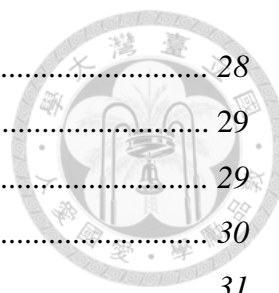
each object. This proposed algorithm effectively decreases time consuming on printing and saves energy consuming furthermore. For subtractive process, the object information can be obtained from additive process and is transformed to subtractive coordinate system. The sculpture region of the 3D object is initially expanded into 2D space by conform mapping, and the vertices of the flattening plane are adjusted to appropriate positions using spring mass model with edge-based flattening algorithm to minimize distortion of flattening plane. Then the 2D image can be intuitively projected onto the expanded plane by geometrical transformation. The projected product in 2D space can be reversely transformed into 3D space, where the reconstructed surface is fitted onto the original surface of the object. Therefore, the subtractive part can run along the path that is generated by above steps. We have demonstrated the success of the proposed methods by using the development of hybrid 3D printing machine consisting of additive and subtractive processes in our NTU robotics and automation lab.

Keywords: three dimensional printing, hybrid 3D printing machine, additive manufacturing, additive and subtractive processes, two dimensional packing problem, traveling salesman problem
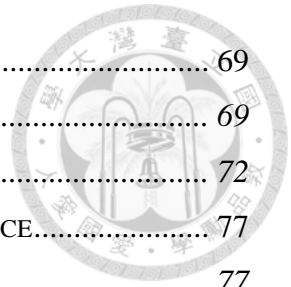
TABLE OF CONTENTS

LIST OF FIGURES

LIST OF TABLES

Chapter 1　Introduction

1.1 Introduction

In the recent years, three dimensional (3D) printing is the fastest growing technologies. Compared with traditional manufacturing techniques, 3D printing has some advantages such as ability of product customization and rapid prototyping, low cost of production, material saving, and ease of designing and manufacturing. Fused Filament Fabrication is a method of the extrusion-based 3D printing. With this method, the thermoplastic material, like Acrylonitrile Butadiene Styrene (ABS) or Poly-Lactic Acid (PLA), becomes gelatinous liquid by heater. Then the material is deposited as the filament through the extruder nozzle which moves along a manufacturing path. However, the extrusion-based 3D printer has limited in manufacturing time which depends on the complexity and size of models.

In nowadays, 3D printing is widely applied in industry, aerospace and medicine, etc. For example, in the aerospace industry, Airbus announced that its new Airbus A350 XWB included over 1000 components manufactured by 3D printing. GE Aviation revealed that it had used design for additive manufacturing to create a helicopter engine with 16 parts instead of 900, with great potential impact on reducing the complexity of supply chains. In the medicine, 3D printing prosthetics are also used for the treatment of injured animals. In the construction industry, the new company, "Apis Cor" in San Francisco, has developed a cost-effective solution to build a house that can be built in less than 24 hours. In the Automotive industry, Local Motors debuted Strati, a functioning vehicle that was entirely 3D Printed using ABS plastic and carbon fiber, except the powertrain.

1.2 Motivation and Objective

The 3D printing technology develops rapidly in the past decades. The 3D printer is based on the technology of additive manufacturing. It builds an object layer by layer so that it can fabricate a very complicated geometrical object.

On the additive process, we focus on the multi-objects printing efficiently. The two key points are mentioned that one is the locations of the multiple objects and another is the times and length of the transition travel. The printing location of the multiple objects directly influences the length of transition path, and then the manufacturing time changes with it. Therefore, planning the location of the objects is significant. On the other hand, we all know that the printer will not move to the next layer until it completes the all machine path on the current layer with traditional 3D printing method. So when the multiple models are printed, the traditional method generally takes much time on the transition travel where the nozzle moves along among the objects without printing. The transition travel is necessary for multiple models but it is so excessive that the process will become inefficient. As a result, minimizing the times and length of the transition travel as much as possible is very important.

On the subtractive process, as the industries and manufacturers having the increasing demands of customized production, such as remarking serial number and carving the logo or brand on the surface product, neither the additive nor subtractive manufacturing can satisfy all the requests individually. However, it is complicated that the logo or brand is designed on curved surface. Therefore, customized logo or trademark is supposed to be displayed on the surface of products, which cannot be completed only by 3D printing techniques. Projection algorithm, which transfers the 2D image to 3D sticker that matches

2

the surface of products, is one of the techniques to satisfy this demand.

In this thesis, we mainly try to solve two problems: the first one is, we minimize the times and length of the transition travel to reduce the production time by planning the location of the multiple objects and adjusting the printing path.

The second one is; the objective of this paper is to describe that hybrid 3D printing approach to carving 2D image on the 3D curved surface based on surface flattening. In addition, the hybrid process combining additive and subtractive processes completes the designed production. The additive process can print main structures of 3D model while the detailed part can be carved by subtractive process. The advantage of cooperation of this method can not only omit repositioning process but also preserve the accuracy of the production.
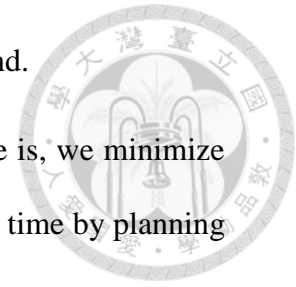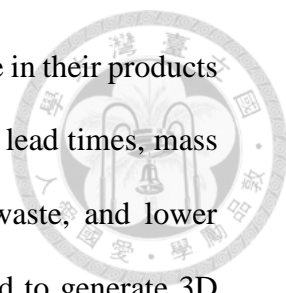
1.3 Literature Review

1.3.1   Flattening Surface

The curved surface of 3D model can be divided into developable and non-developable surface. The developable surface with zero Gaussian curvature can be flattened onto a plane without distortion such as cylinders, cones and so on. Another surface has double curvature and non-zero Gaussian curvature such as spheres, helicoid, etc. [1] and [2] focus on multi-objective optimization problem (MOPs). The non-dominated sorting adaptive differential evolution (NSJADE) and cooperative coevolutionary multi-objective evolutionary algorithms (CCMOEAs) are proposed respectively. In [3] [4], use the conformal function to do flattening process, but only solve the simply-connected and low curvature. The angle based flattening (ABF) method [5] [6] uses angles of triangle on the surface mesh as optimized parameters. The optimized parameters are so many that ABF is usually inefficient. The edge based flattening (EBF) method [7] computed the parameterization of flattening plane for minimal distortion. And [8] presented a flattening method based on a mass spring model.   A model-based surface approximation method for three-dimensional (3D) surface quality inspection is proposed in [9]. It combines a machine learning approach with multiresolution paradigms to automatically determine the area of local refinement.

1.3.2   Additive Process

Additive manufacturing (AM) or three-dimensional (3D) printing is a technique that is used to fabricate products and components from digital models layer-by-layer.

4

Because of its potential, various industries have applied this technique in their products manufacturing. There are many benefits of AM including shortening lead times, mass customization, printing more complex shapes, reducing material waste, and lower energy consumption. The paper [10] introduces an enhanced method to generate 3D prints of individual joining gaps in the automated assembly. A detailed overview of additive manufacturing applications in the industries presented in the [11], focusing on the likely effects on organizations and, moreover, to emphasize and discuss the potential of this technology in the field of the industrial value chain.

Furthermore, additive manufacturing is often used in customized production as well, especially in the medical field. In [12], an EOS M-type direct metal laser sintering (DMLS) system is used to manufacture some customized hip implant with an IPG fiber laser using titanium alloy.

A new digitally driven hybrid fabrication process chain, which can produce functional, multilayer electronics embedded within geometrically complex 3D printed structures, are proposed in [13].

1.3.3   Subtractive Process

Subtractive manufacturing has been widely used in modern manufacturing industry with the diverse characteristics of high brightness, high directivity and high coherence such as deburring, cutting, welding, marking and carving. Laser cutting, one of the most used subtractive manufacturing methods, is widely used in aviation, electronics, automobile, machinery manufacturing and other industrial fields. A new real-time rotation-invariant template matching is proposed for industrial laser cutting applications in [14]. In [15], the authors design a new cutting method with the improved

5

accuracy and speed of small hole laser cutting.

1.3.4 Path Generation and Planning

We all know that the quality of products depends on path generation. Its procedure is generating a set of points distributed according to the gray image and constructing a continuous path through the points for guiding material deposition in [16]. [17] develops an algorithm that is capable of processing and slicing an STL file or multiple STL files plans the path of the tool and finally generats a G-code file for an entry level 3-D printer.

The total manufacturing time is relative to the quality of path planning. Trajectory modifications are encoded in particles that are optimized by using particle swarm optimization (PSO) to solve motion planning problems with complex constraints in [18]. In paper [19], the MZZ-GA algorithm combines the modified zig-zag (MZZ) and genetic algorithm (GA) to improve the path optimization. In paper [20], it shows how to generate G-code by slicing software (obtained with Slic3r). Then the G-code is analyzed to extract local features of an object in order to reduce the transition travel. The optimized motion paths of the printing nozzle based on Christofides algorithm is proposed in [21]. The paper [22] provides an $O(n \log n)$ time   algorithm that combines an improved Dijkstra's algorithm and the concept of ridge points to build a connected graph. The length of shortest possible path on the polygonal surface is obtained by the graph. On the other hand, motion control is discussed to optimize the motion speed as well as minimize the transition time the paper [23]. [24] uses the genetic algorithm (GA) and the particle swarm optimization algorithm to solve the complexity of the problem and obtains the feasible and quasi-optimal trajectories. A linear segment with

6

parabolic blends (LSPBs) trajectory planning algorithm and minimum time trajectory (MTT) are used to improve the printing performance in [25]. The paper [26] presents two different algorithms and both reduce the distance in the path planning. One is a simple greedy method that uses the heuristic function to create the path as short as possible. The other is based on the combination of the nearest and the farthest insertion method. The results of first algorithm is better when there are a few contours. However, as the number of contours increases, the second algorithm performs better.

1.4 Additive Manufacturing methods

Additive manufacturing (AM), also known as 3D printing, is a method that builds a three-dimensional model of rapid prototyping and product in a customization fashion. The STL file of 3D model needs to be processed by slicing software, which converts the model into a series of layers and outputs the "G-code" file containing the instructions about temperature of heat, speed of nozzle motion, velocity of the stepper motor, and so on. Therefore, additive manufacturing technologies not only reduce the new product development cycle, but also allow users to design models of their own style.

Next, we will introduce the many different aspects of the practice in additive manufacturing. The main differences between processes are in the way that layers are deposited to build up the models and in the materials that are used.

1.4.1   Fused Deposition Modeling (FDM)

Fused deposition modeling, also known as fused filament fabrication (FFF) in Figure 1.4-1, is an additive manufacturing technology commonly used to build up the 3D models.

FDM process is that a plastic filament supplies material to a temperature-controlled head and is heated to melt the material. Then the extrusion nozzle can moved in both horizontal and vertical directions by a numerically controlled mechanism and extrude a thermoplastic material layer by layer onto a workspace. Finally, the fused material is deposited layer by layer to build up the models.
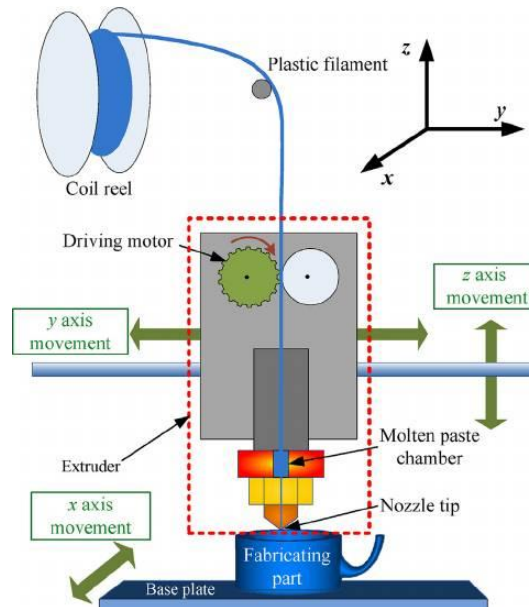
Figure 1.4-1 The illustration of fused filament fabrication
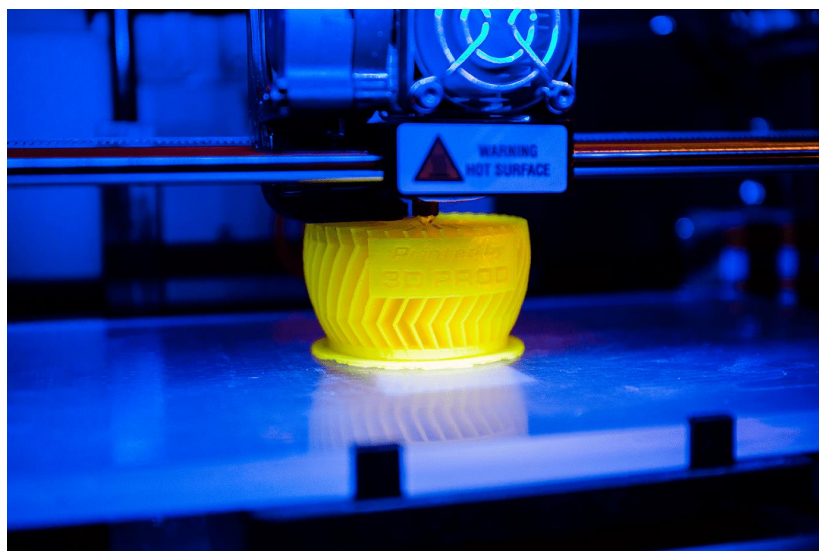
Figure 1.4-2 Fused filament fabrication

8

1.4.2   Stereo Lithography Apparatus (SLA) / Digital Light Processing (DLP)

The production procedure is done in a layer by layer fashion using photopolymerization, and it is a process by which light causes chains of molecules to link, forming polymers. In other words, using a light source (e.g. UV laser or projector) to cure liquid resin into hardened plastic. Those hardened plastics can construct the three dimensional entity step by step.
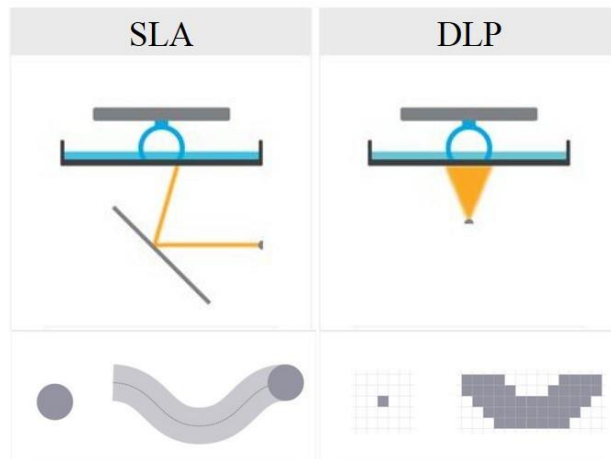
Figure 1.4-3 Compare the difference between SLA and DLP. SLA : selective exposure to light from laser. DLP : selective exposure to light from projector.
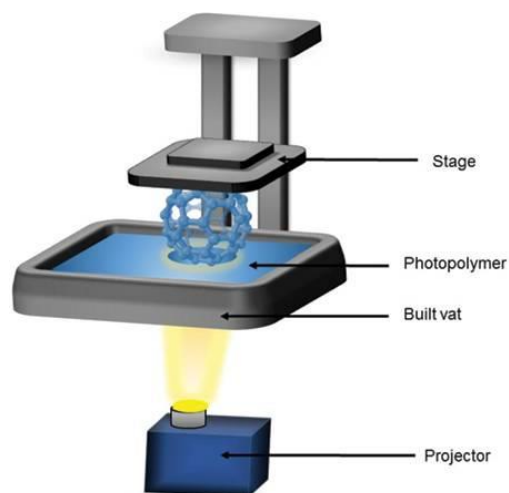
Figure 1.4-4 The illustration of Digital light processing (DLP)

9

Figure 1.4-5 The printing process of running shoe

1.4.3 Selective laser sintering (SLS)

A laser beam which is controlled by computer selectively fuses powdered material by scanning X and Y cross-sections on the surface of a powder bed. Using the laser as the power source to sinter powdered material binds the material together to create the three dimensional structure. Once the first layer is formed, the platform will drop usually by less than 0.1 mm and expose a new powder layer for the laser to fuse together. This process will continue again and again until the model has been completed.
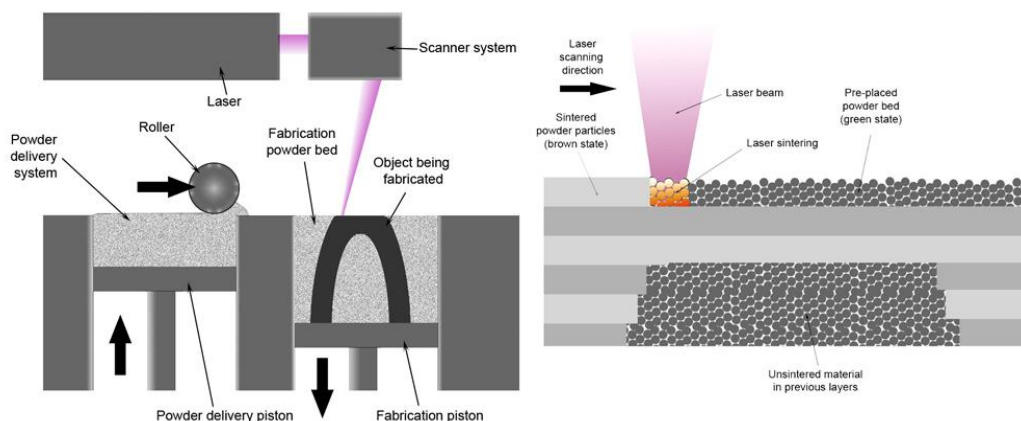
Figure 1.4-6 The illustration of selective laser sintering

10
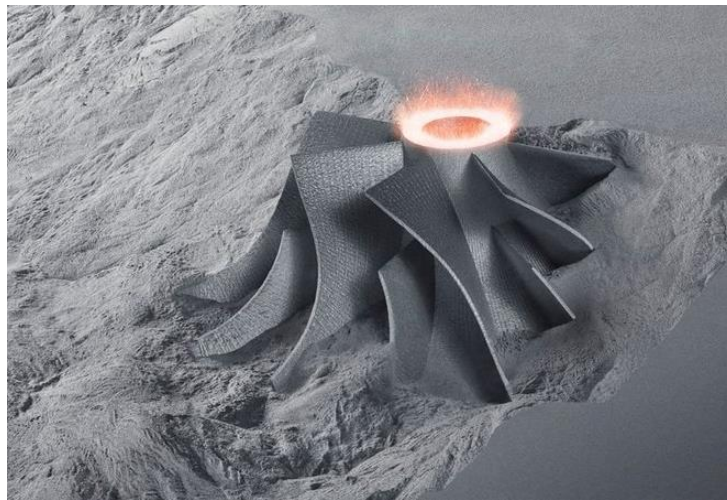
Figure 1.4-7 The result of selective laser sintering

1.4.4   Selective laser melting (SLM)

Another method of 3D metal printing is selective laser melting (SLM), in which a high-powered laser fully melts each layer of metal powder rather than just sintering it. Selective laser melting produces printed objects that are extremely dense and strong.
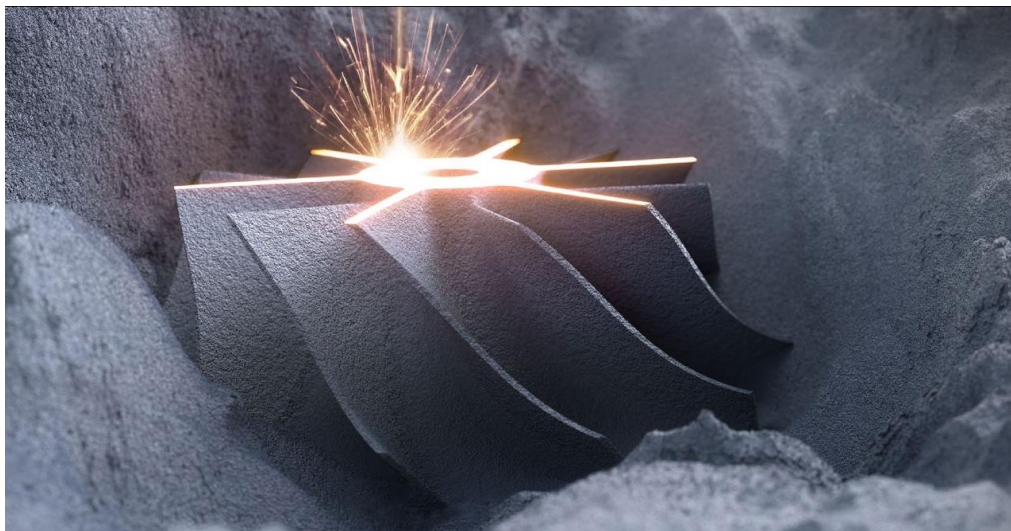
Figure 1.4-8 The result of selective laser melting

1.4.5   Laser metal deposition (LMD)

Laser metal deposition (LMD) is an additive manufacturing process in which a laser beam forms a melt pool on a metallic substrate, into which powder is fed. The powder melts to form a deposit that is fusion-bonded to the substrate. The required model or geometry is built up in this way, layer by layer. Both the laser nozzle head can be manipulated using a gantry system or robotic arm.
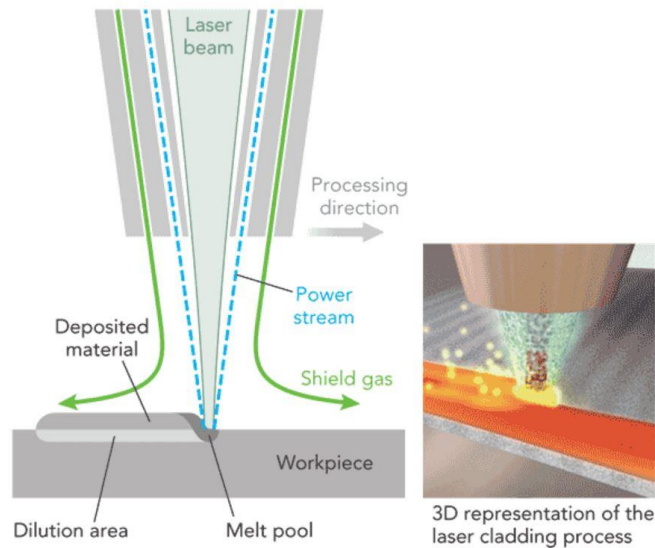
Figure 1.4-9 the illustration of laser metal deposition (LMD)
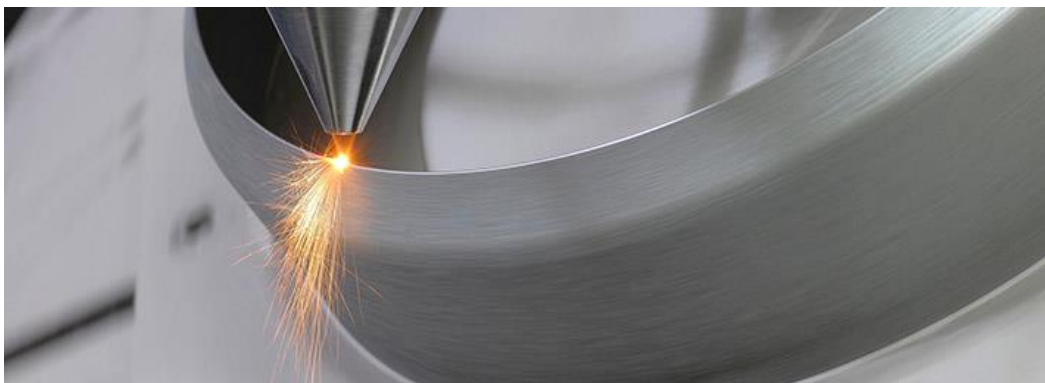
Figure 1.4-10 Laser metal deposition (LMD)

12

1.4.6 Compare with additive manufacturing methods

Table 1 Compare with additive manufacturing methods

	Material	Advantages	Disadvantages
FDM	1. PLA (Polylactic Acid) 2. ABS (Acrylonitrile Butadiene Styrene) 3. Nylon 4. Wax	1. Low maintenance costs 2. Equipment costs are inexpensive 3. The price of material is inexpensive	1. Axial strength is weak 2. Low accuracy 3. The surface has a step structure 4. Need supports
SLA	1. Light-Curing Resins	1. Excellent surface quality 2. No need supports	1. Fewer types of materials can be used 2. The price of resin material is expensive
SLS	1. Nylon 2. Polystyrene, 3. Metals including steel, titanium, alloy mixtures, and composites 4. Green sand	1. Various types of materials can be used 2. No need supports 3. high accuracy	1. The surface roughness is granulated 2. Need post-processing 3. Expensive high power laser 4. Dust pollution
SLM	1. Most metals including copper, aluminium, stainless steel, toll steel, cobalt chrome, titanium and tungsten.	1. Structural strength is high 2. No need supports 3. high accuracy	1. Expensive high power laser 2. Dust pollution 3. Expensive high power laser
LMD	1. Most metals including titanium alloy, copper, aluminium,	1. Achieve rapid repair of damaged parts 2. high accuracy	1. Expensive high power laser

13

	stainless steel, toll steel, cobalt chrome and tungsten.	3. the head can be manipulated using a gantry system or robotic arm	

1.5 Thesis Organization

The thesis is organized as follows. Following this introduction, the experimental equipment and the 3D printer machine developed in our NTU-iCeiRA laboratory are introduced in Chapter 2. The hardware and software architectures are illustrated in the chapter. Moreover, the printing material is specified here. In Chapter 3 and Chapter 4, the highlighted processes in the additive and subtractive manufacturing are elaborated in detail. The additive manufacturing for multiple heterogeneous objects is discussed in Chapter 3. The fabrication procedures are illustrated in order, from the model extraction and analysis, collision consideration, printing strategy evaluation and planning location of multiple objects. In Chapter 4, carving 2D image onto 3D curved surface using hybrid additive and subtractive 3D printing approach is fully described. The proposed surface flattening algorithm that combines conformal mapping with optimal adjuster based on edge-lengths of the original mesh is illustrated. In Chapter 5, the experimental results about multiple heterogeneous objects fabrication and carving process are conducted on the 3D printer machine developed in our NTU-iCeiRA laboratory to evaluate the feasibilities of the proposed system. Analysis on the experimental results is also carried out to verify the proposed algorithms. Finally, the conclusions and future work are presented in Chapter 6.

Chapter 2   The Hardware and Software

2.1 Hardware

2.1.1   Mechanism Design
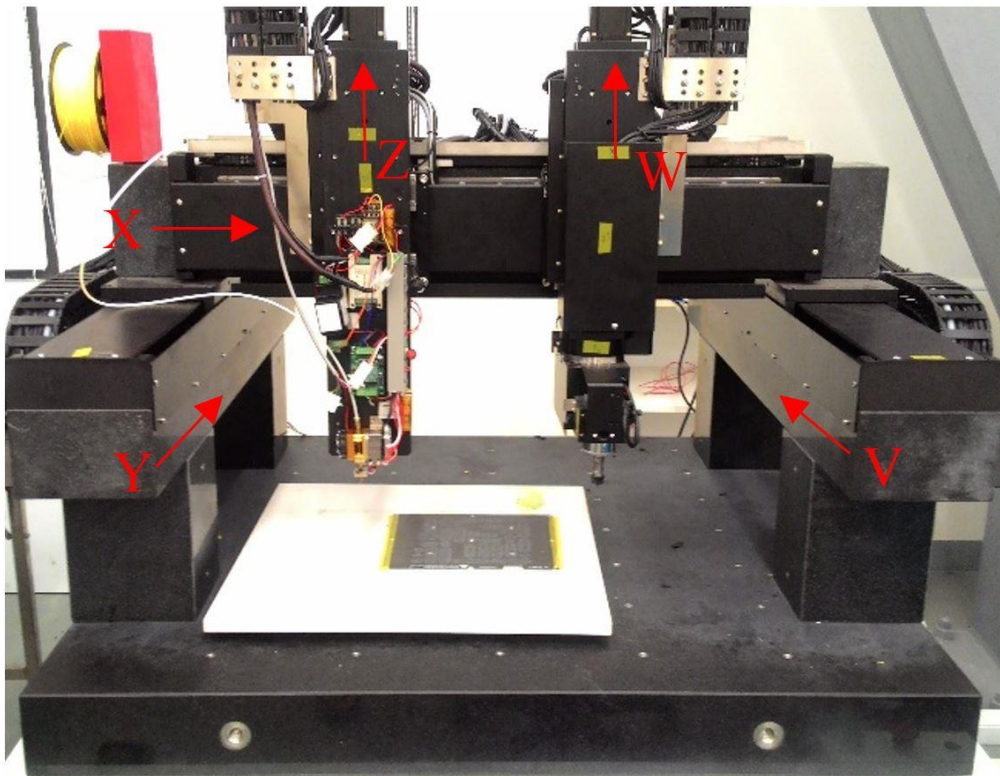
Figure 2.1-1 There are two parts on the gantry-type hybrid machine. Left side is the additive (3D printing) part while right side is subtractive (cutting) part.

Both 3D printer and cutting tool are integrated in the gantry-type hybrid machine in Figure 2.1-1. The "hybrid" means that the printing part and carving part cooperate to complete the products. The machine not only executes additive and subtractive process separately but also combines two parts to do remanufacturing procedures of the same product. The cooperation can improve the accuracy of the production and the

15

repositioning process can be omitted at the same time.

2.1.2   Robot Coordinate System

The Denavit–Hartenberg parameters (D-H parameters) are the four parameters associated with a particular convention for attaching reference frames to the links of a spatial kinematic chain, or robot manipulator. Jacques Denavit and Richard Hartenberg introduced this convention in 1955 in order to standardize the coordinate frames for spatial linkages. The four parameters are necessary to fully describe the relationship between adjacent links and joints as follows:

D-H parameters in terms of the link frames:

- d_i : the distance from $\hat{x}_{i-1}$ to $\hat{x}_i$ measured along $\hat{z}_{i-1}$

- θ_i : the angle from $\hat{x}_{i-1}$ to $\hat{x}_i$ measured about $\hat{z}_{i-1}$

- a_i : the distance from $\hat{z}_{i-1}$ to $\hat{z}_i$ measured along $\hat{x}_i$

- α_i : the angle from $\hat{z}_{i-1}$ to $\hat{z}_i$ measured about $\hat{x}_i$

The procedures for attaching coordinate on the link and identifying these four parameters are described as follows:

Link frame attachment procedures:

1. Identify the joint axes and imagine (or draw) infinite lines along them. For steps 2 through 5 below, consider two of these adjacent lines (at i^{th} and $i+1^{th}$ axes).

2. Identify the common perpendicular between them, or point of intersection. At the point of intersection, or at the point where the common perpendicular meets

16

the ith axis, assign the link-frame as origin.

3. Assign the $\hat{z}_{i-1}$ axis pointing along the ith joint axis.

4. Assign the $\hat{x}_{i-1}$ axis pointing along the common perpendicular, or, if the axes intersect, assign $\hat{x}_{i-1}$ to be the normal to the plane containing the two axes.

5. Assign the $\hat{y}_{i-1}$ axis to complete a right-hand coordinate system.

6. Assign frame $\{0\}$ anywhere in the base as long as the $\hat{z}_0$ axis lies along the axis of motion of the first joint. The last coordinate (frame $\{n\}$) can be place anywhere in the end-effector as long as the $\hat{x}_n$ axis is normal to the $\hat{z}_{n-1}$ axis.

7. Try to assign the link frame so as to cause as many linkage parameters as possible to become zero.
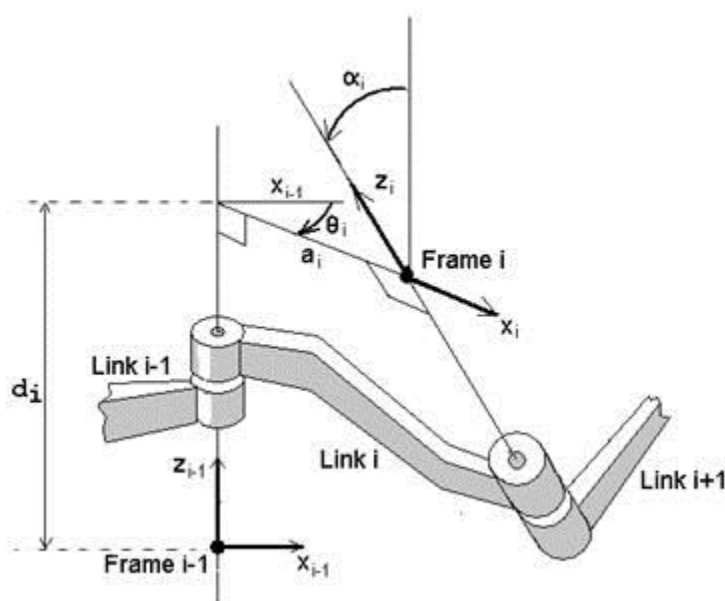
Figure 2.1-2 Definition of the D-H parameters

2.1.3　System Structure
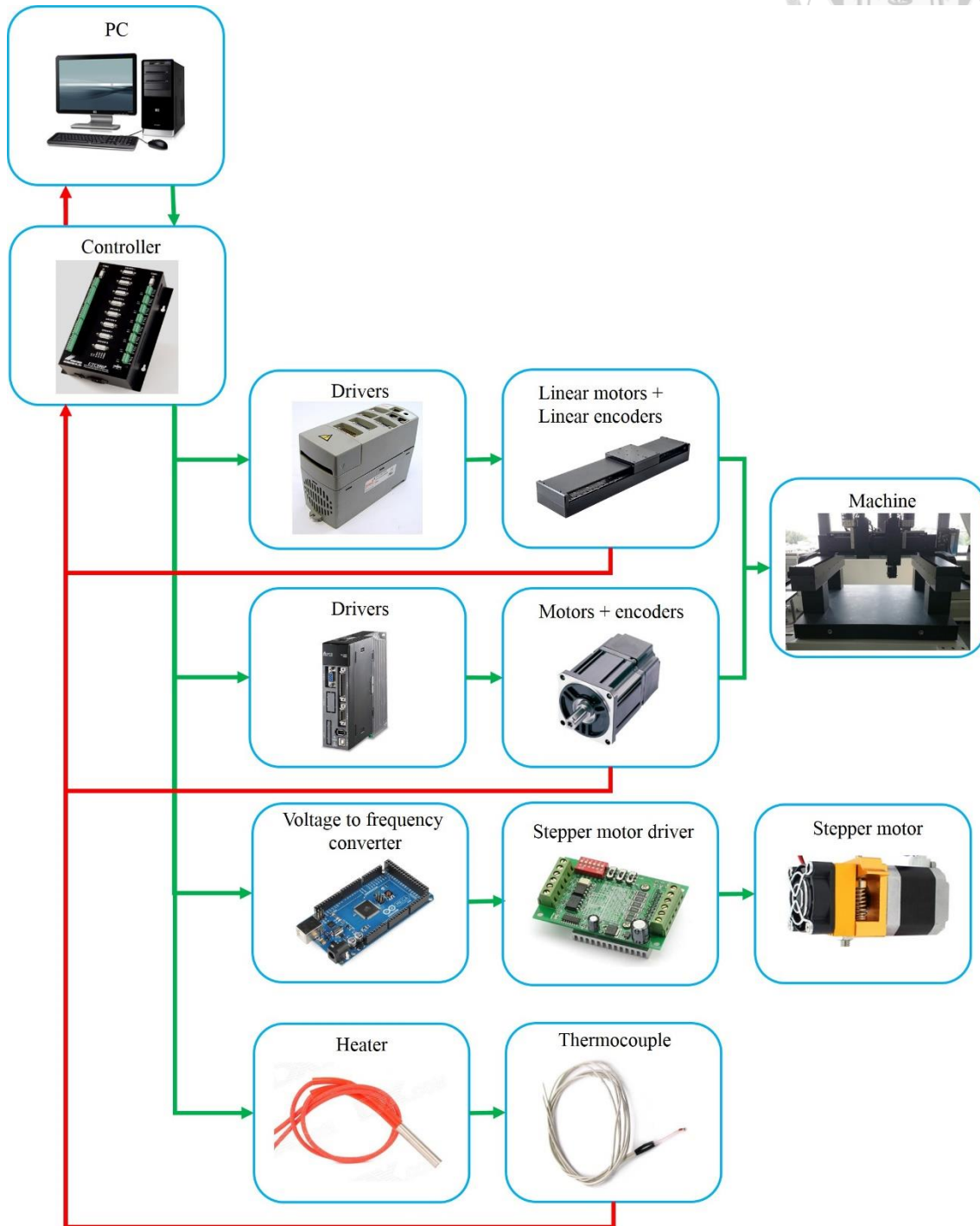
Figure 2.1-3 Control architecture

18
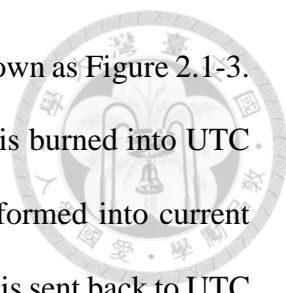
The control architecture of the gantry-type machine system is shown as Figure 2.1-3. The algorithm program is developed in PC base, then the algorithm is burned into UTC controller. And the voltage signal is sent into the driver to be transformed into current signal. While the machine is executing, the angle signal from encoder is sent back to UTC controller to achieve the feedback control. On the 3D printer part, the UTC controller also controls the speed of stepper motor and heater.

- Controller (UTC800P)

We use UTC controller as our operating kernel to manipulate the machine and implement the proposed algorithms. This controller provides some functions to control the machine smoothly and efficiently. Table 2 shows the specifications of controller, and the functions that contain communication, AD/DA(PWM), DNC, Blended Move and so on are often used.
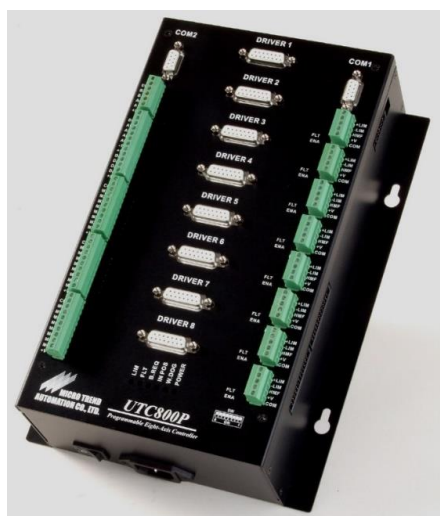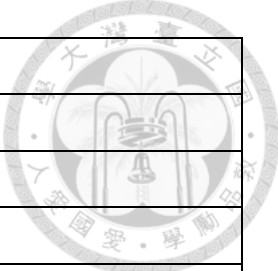
Figure 2.1-4 UTC controller

Table 2 Specifications of UTC controller

Specifications	UTC800V/P
CPU	TMS320C32
Number of Control Axes	8

Driver	(excluded)
Command Out	8V(16bit) / 8P(2M)
PLC/Motion Program	16 / 256 units
Communication	RS-232x2/USB
Multi-Coordinate System	8
Look Ahead	1
Servo Algorithm	PID+FF/ by Driver
Electrical Gear/Cam	Table / Time base
On Board DI/DO	16 in / 8 out
AD/DA(PWM)	4(16bit)/4(12bit)
RAM	4Mb(16Mb)
Back Up RAM 4Mb	Battery+Flash
System Clock Frequency (Hz)	40M
Servo Update Rate	1ms
Cutter Radius/ Lead screw Compensation	N
Dual Encoder Feedback	Y
DNC	Y
Timers/Variables	8 / 4096
Hardware Capture Function	Y
Password Security	Y
Linear/Circular/ Screw Interpolation	Y
Cubic Spline Interpolation	Y
Scaling & Rotation	Y
Blended Move	Y
User-Defined G/M Code	Y

● Controller (Arduino MEGA 2560)

This small controller is used as voltage to frequency converter to analyze the voltage

signal of UTC controller, and will transform the voltage signal into the corresponding

frequency output. The stepper motor driver needs to the clock to control the speed of

20

motor, but the UTC controller has only the voltage signal and it cannot output the different frequency. Therefore, we need the converter to transfer voltage into frequency signal. In the specifications, the digital I/O pins and analog input pins are often used with Arduino library.
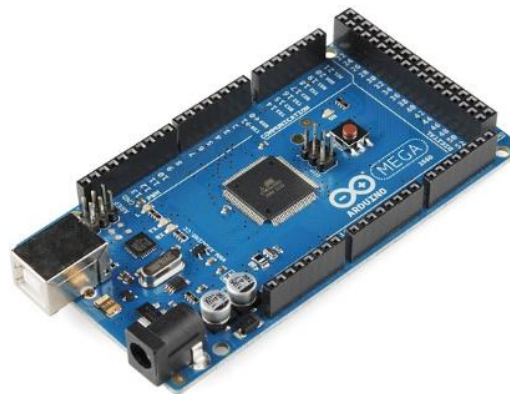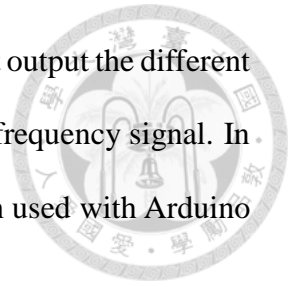
Figure 2.1-5 Arduino MEGA 2560

Table 3 Specifications of Arduino MEGA 2560

Microcontroller	ATmega2560
Operating Voltage	5V
Input Voltage (recommended)	7-12V
Input Voltage (limit)	6-20V
Digital I/O Pins	54 (of which 15 provide PWM output)
Analog Input Pins	16
DC Current per I/O Pin	20 mA
DC Current for 3.3V Pin	50 mA
Flash Memory	256 KB of which 8 KB used by bootloader
SRAM	8 KB
EEPROM	4 KB
Clock Speed	16 MHz
LED_BUILTIN	13
Length	101.52 mm
Width	53.3 mm
Weight	37 g

21

● Stepper Motor Driver (TB6560)

This driver can control the speed and direction of the stepper motor. The different position of dip switches have the different outputs. In the experiment, the running current that should be lower than the current rating of motor is set as 1.5A and the stop current is 50%. Excitation mode and decay setting are set as 1/16 and 0% respectively. The excitation mode can be said to be the resolution of the stepper motor. Therefore, excitation mode is set as a smaller value to let motor run smoothly.
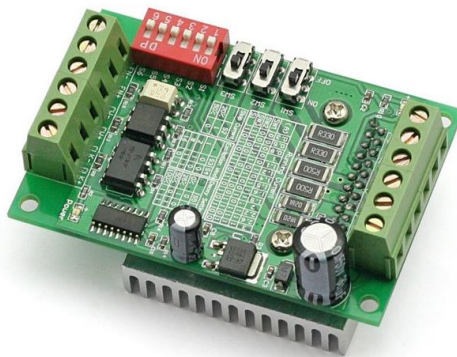
Figure 2.1-6 stepper motor driver

Note :

1. 6 input terminals can be connected as common anode or cathode.

2. The normal input voltage is if it is more than 5V, than a series resistor is needed. This resistance is 1K case 12V and 2.4K case 24V.

3. When pulse is applied to CLK, the stepping motor will rotate, and stop when there is none, and the motor driver will change its current to the half mode as setting to hold the motor still.

4. Motor rotate clockwise when CW is low level and counterclockwise when CW is high level.

5. Motor is enable when EN is low level and disable when EN is high level.

22
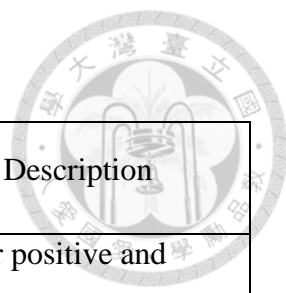
Table 4 Pins introduction of driver

	Wiring Terminal symbol	Description
	+24V, GND	Power positive and negative
	A+, A-	Motor phase A
	B+, B-	Motor phase B
	CLK+, CLK-	Pulse positive and negative
	CW+, CW-	Direction positive and negative
	EN+, EN-	Enable positive and negative

Table 5 Running current setting

Running Current														
(A)	0.3	0.5	0.8	1	1.1	1.2	1.4	1.5	1.6	1.9	2	2.2	2.6	3
SW1	X	X	X	X	X	O	X	O	O	O	O	O	O	O
SW2	X	X	O	O	O	X	O	X	X	O	X	O	O	O
SW3	O	O	X	X	O	X	O	O	X	X	O	O	X	O
S1	O	X	O	X	O	O	X	O	X	O	X	O	X	X

(X : OFF   O : ON)

Table 6 the setting about stop current, excitation mode and decay setting

Stop Current		Excitation Mode			Decay Setting		
	S2	Step	S3	S4	Step	S5	S6
20%	ON	Whole	OFF	OFF	0%	OFF	OFF
50%	OFF	Half	ON	OFF	25%	ON	OFF

		1/8	ON	ON	50%	ON	ON
		1/16	OFF	ON	100%	OFF	ON
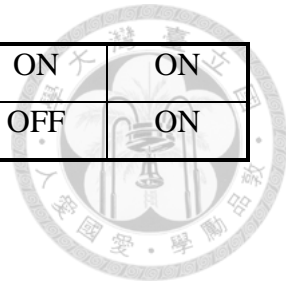
- Stepper Motor

A stepper motor, also known as step motor or stepping motor, is a brushless DC electric motor, and the motor's position can then be commanded to move and hold at one of these steps without any feedback sensor. Its property to convert input pulses into the increment in the shaft position. Each pulse drives stepper motor to move a fixed angle that is depended on excitation mode of motor driver.

Figure 2.1-7 Stepper Motor

2.2 Software

2.2.1 STL (STereoLithography) Format

3D print models are typically distributed in a file format called STL. An STL file describes a raw unstructured triangulated surface by the unit normal and vertices (ordered by the right-hand rule) of the triangles using a three-dimensional Cartesian coordinate system. As a general rule, changing options such as chord tolerance or angular control will change the resolution on the STL file (see figure (b) and (c)).

24

STL-file

solid *name*

$$\left\{\begin{array}{l} \text{facet normal } \; n_i \;\; n_j \;\; n_k \\ \quad \text{outer loop} \\ \qquad \left.\begin{array}{l} \text{vertex } \; v1 \;\; v1 \;\; v1 \\ \text{vertex } \; v2 \;\; v2 \;\; v2 \\ \text{vertex } \; v3 \;\; v3 \;\; v3 \end{array}\right\} \\ \quad \text{endloop} \\ \text{endfacet} \end{array}\right.$$

endsolid *name*
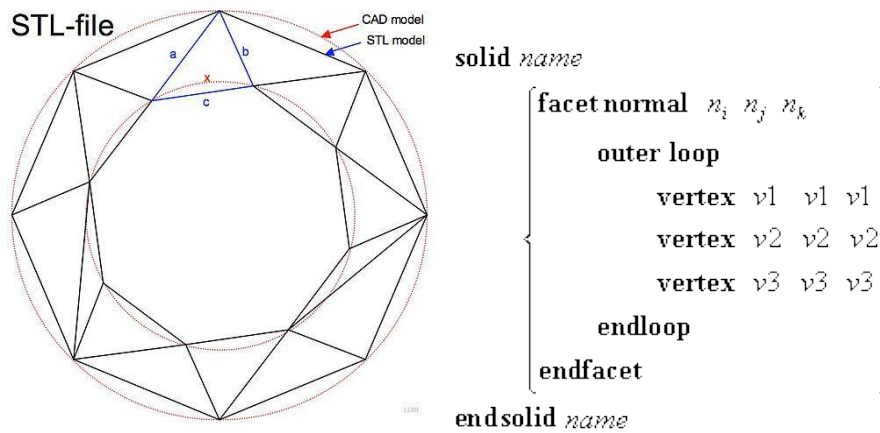
Figure 2.2-1 STL file and format

(a)   (b)   (c)
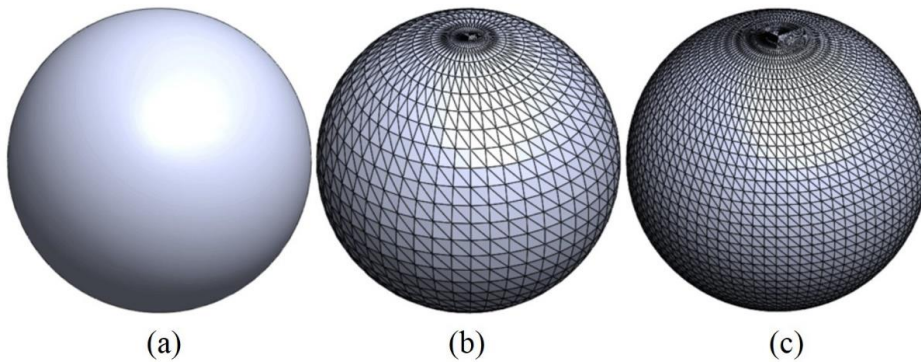
Figure 2.2-2 (a) CAD model (b) STL format (c) higher resolution STL format

2.2.2   Slicing Software

The process from the 3D file into the entity needs to do slicing processing step, and this step usually is implemented by slicing software or slicer. The slicing software takes 3D files (STL) and generates path information (G-Code) for a 3D Printer. These paths are written in G-Code, a program language, which describes the coordinates and instructions of the 3D printer's nozzle when moving.

25
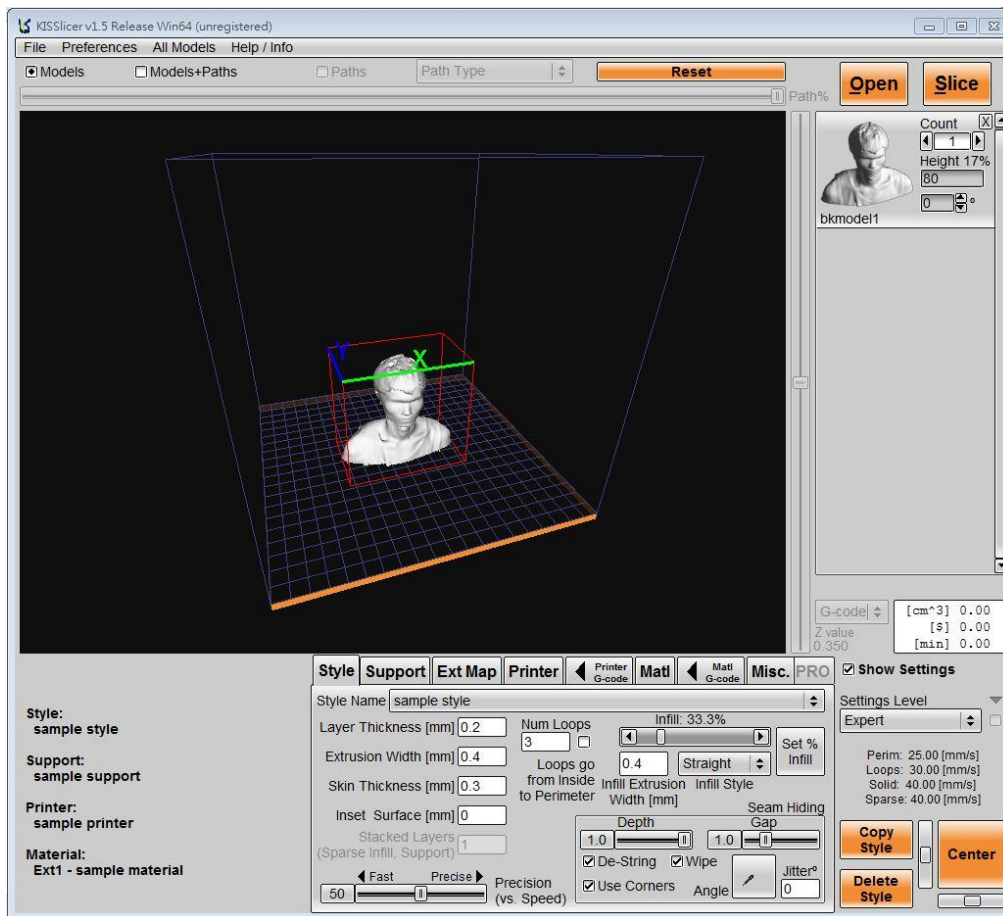
Figure 2.2-3 KISSlicer slicing software [27]

Table 7 the basic setting in the slicing software

Instructions	Description
Layer Height / Layer Thickness (unit : mm)	Layer thickness is a measure of the height of each successive addition of material in the additive manufacturing or 3D printing process in which layers are stacked. It is one of the essential technical characteristics of every 3D printer; the layer thickness is essentially the resolution of the z-axis, which is the vertical axis. If the sitting of layer thickness is smaller, the printed is more detailed and the higher the quality of the model but the longer the printing time.
Skin Thickness (unit : mm)	Whether the top, bottom, or side thickness of the model will be greater than or equal to this setting. The slicing software

26

	automatically calculates the number of top and bottom layers, as well as the thickness of the outer contours, to satisfy the thickness settings.
Fill Density / infill (unit : %)	It is the density of the inside of the 3D print object. If the fill density is 100%, then the model will be printed as solid, and 0% represents that model will be hollow.
Print Speed (unit : mm/s)	The nozzle head moves at certain velocity when printing the material. The sitting of speed can be obtained by trial and error method to get the appropriate print speed.
Support	This allows a model to be built up to angles of 45°, allowing prints to expand beyond its previous layer's width. When a feature is printed with an overhang beyond 45°, it can sag and requires support material beneath it to hold it up.
Printing Temperature (unit : ℃)	Each print material such as PLA or ABS has a temperature range in which nozzle can be printed smoothly. Too high or too low nozzle heating temperature affects print quality. The heating temperature of PLA is generally about 210 to 225 degrees, while the ABS is about 230-245 degrees.

G-Code format

```
G1 X104 Y104.61 Z0.7 E0 F30000
G1 X104 Y104.61 Z0.45 E0 F210
G1 E1.25 F900
G1 X103.25 Y105.22 E0.109 F600
G1 X102.13 Y105.5 E0.1295
G1 X97.55 Y105.49 E0.5139
G1 X96.43 Y105.03 E0.1365
G1 X94.95 Y103.55 E0.2344
```

Figure 2.2-4 G-Code file

Table 8 the common G-Code in 3D printers
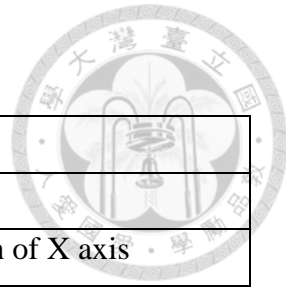
Code/ Variable	Description
G1	Linear move
X	Absolute or incremental position of X axis
Y	Absolute or incremental position of Y axis
Z	Absolute or incremental position of Z axis
E	material length of extruding (mm)
F	motion speed (mm/min)
For example	
G1 X102.13 Y105.5 E0.1295	Move to 102.13mm on the X axis and 105.5mm on the Y axis while extruding 0.1295mm of material.

2.2.3   Direct Numerical Control (DNC)

Direct numerical control (DNC), also known as distributed numerical control, is a common manufacturing term for networking CNC machine tools. On some CNC machine controllers, the available memory is too small to contain the machining program, so in this case the program is stored in a separate computer and sent directly to the machine. With a direct numerical control system, the program will be run from a device (commonly a PC) connected to the machine's communications port (the RS-232 port). In our system, the MATLAB is used in the host computer communicates with controller through the RS-232 serial port. The computer will ask the controller how many instructions in the memory. If the numbers of instructions in the memory are less than the critical value, the computer will send the following program to the controller. In this way, the controller can keep the amount of instructions to let the machine operate properly.

Number of program lines

UTC
controller

PC
(instructions)

Program instructions
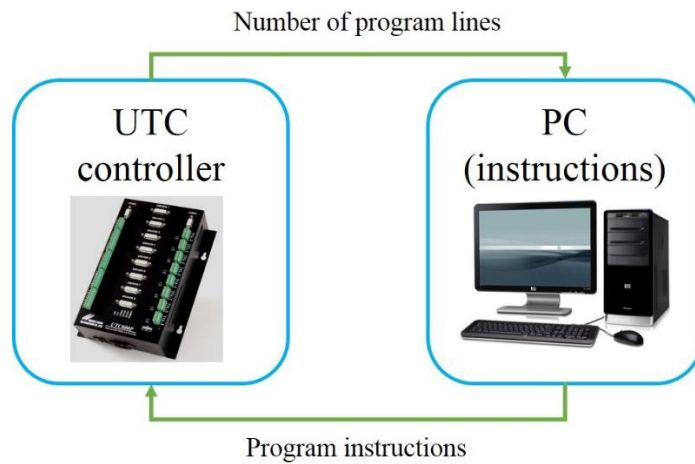
Figure 2.2-5 Direct numerical control

2.3 Material

2.3.1   PLA (Polylactic Acid)

Poly(lactic acid) or polylactic acid or polylactide (PLA) is a biodegradable and bioactive thermoplastic aliphatic polyester refined from renewable resources, such as corn starch (in the United States and Canada), tapioca roots, chips or starch (mostly in Asia), or sugarcane (in the rest of the world). This is why it is called "the green plastic". It's widely used for packaging, such as food products, but of course you can also use it to print. In 2010, PLA had the second highest consumption volume of any bioplastic of the world.

29

Figure 2.3-1 PLA (Polylactic Acid)

2.3.2 ABS (Acrylonitrile Butadiene Styrene)

The most important mechanical properties of ABS are impact resistance and toughness. A variety of modifications can be made to improve impact resistance, toughness, and heat resistance. The impact resistance can be amplified by increasing the proportions of polybutadiene in relation to styrene and also acrylonitrile, although this causes changes in other properties. Impact resistance does not fall off rapidly at lower temperatures. Stability under load is excellent with limited loads. Thus, by changing the proportions of its components, ABS can be prepared in different grades. Two major categories could be ABS for extrusion and ABS for injection moulding, then good impact resistance. For the majority of applications, ABS can be used between −20 and 80 °C (−4 and 176 °F) as its mechanical properties vary with temperature.

30

Figure 2.3-2 ABS (Acrylonitrile Butadiene Styrene)

2.3.3 PLA vs. ABS

Table 9 the difference between PLA and ABS

	PLA	ABS
Print temperature	190~220℃	230~250℃
Plastic source	Corn starch	Petroleum extraction
Material hardness	Strong hardness	High toughness
Fumes and smell	Smells sweet	Hot plastic fumes
Degradability and durability	Biodegradable	Not biodegradable but can be easily recycled
Heated bed	Not necessary	Necessary

Chapter 3 Multi-Heterogeneous Objects

Fabrication for Additive Process

3.1 System Structure
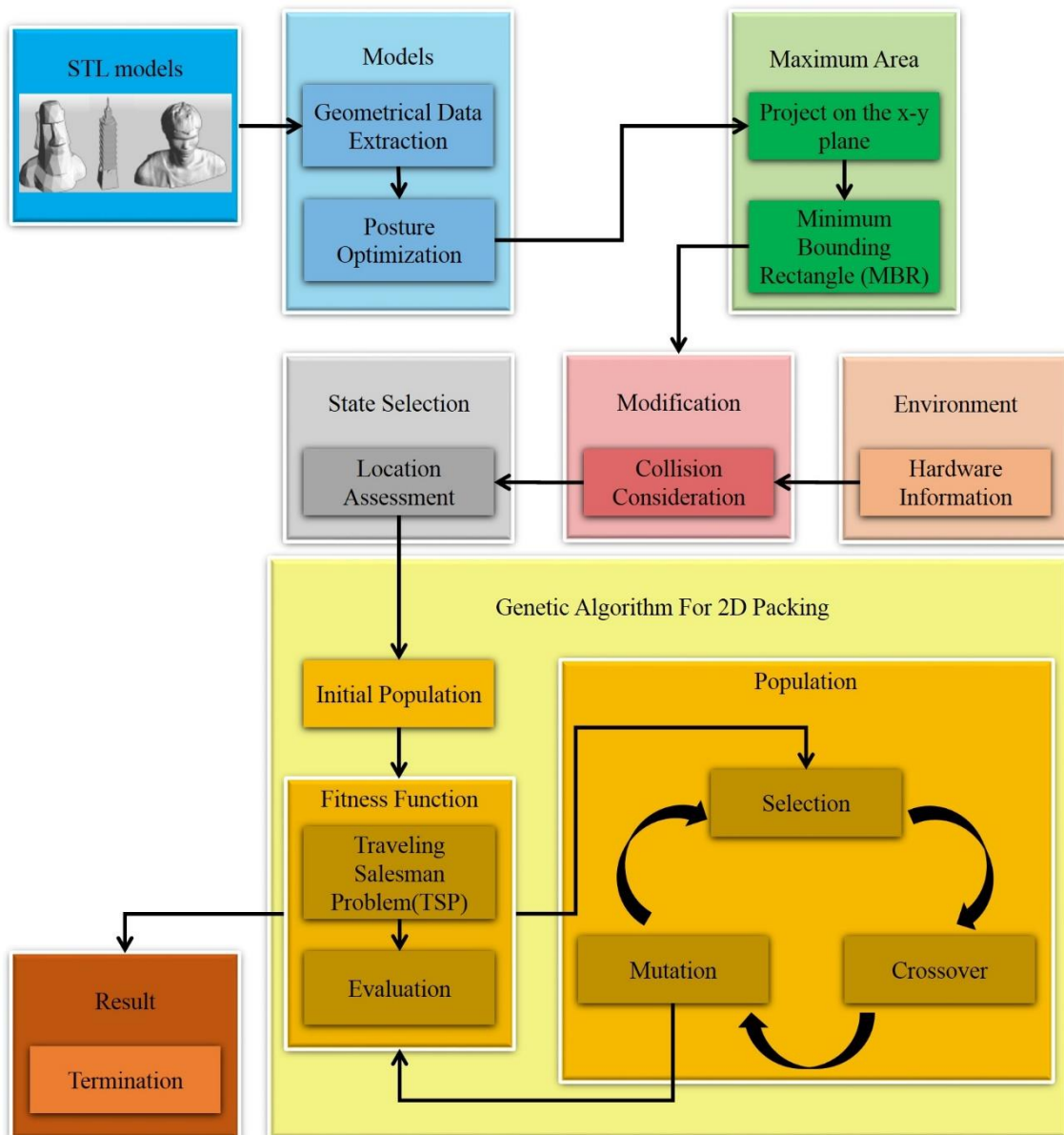
Figure 3.1-1 system flowchart of additive manufacturing for multiple objects

The system can be distinguished into major four steps as follows.

- Step I. Model extraction and analysis

  Each model is adjusted to appropriate posture after the STL file is imported.

- Step II. Collision consideration

  This step needs to consider hardware specification to plan the printing path. The nozzle can avoid colliding with the printed parts.

- Step III. Printing strategy evaluation

  Calculate the relationship between models and workspace to determine the printing strategy. There are three strategies in the printing procedure.

  Case 1: print the model layer by layer.

  Case 2: print the model part by part.

  Case 3: the workspace is large enough. Complete a model before move to the next one.

- Step IV. Planning location of multiple objects

  Using the genetic algorithm solves the 2D packing problem to obtain the optimal solution.

3.2 Model Extraction and Analysis

In the additive manufacturing process, the construction of the support structure is necessary for some complex models. There are several reasons: on the one hand, support the structure of the object and enhance the structure stability between parts and build platforms. On the other hand, the support structure can prevent parts warping and reduce the failure rate in the printing process. Indeed, no one likes to support the structure because it not only affects the production of production and costs, but also

increases the additional printing time, cost, post-processing time and complexity. Therefore, the optimization of the support structure is very important issue in 3D printing. To minimize and avoid the excessive use of the support structure as much as possible, it is necessary to have a good understanding about the geometry of the parts and the limitations of their construction.

For instance, the posture of model can be changed by rotating along the X, Y and Z axis (e.g. roll, pitch, yaw) to obtain proper position. In Figure 3.2-1and Figure 3.2-2, it is a simple case for us to easily comprehend the how to minimize and avoid the extra support structure. There are many support structures (the gray area in the Figure 3.2-1) under the table. The table is rotated 180 degrees along the X or Y axis to obtain the different result (see Figure 3.2-2), and support is not required to build up in the printing process. In the production time, the former needs to take 43.38 minutes to complete, while the latter only takes 30.95 minutes. Comparison between the two can be observed that the latter reduces the use of material and saves the 40.162% production time. Therefore, the support optimization makes printing process more efficient.
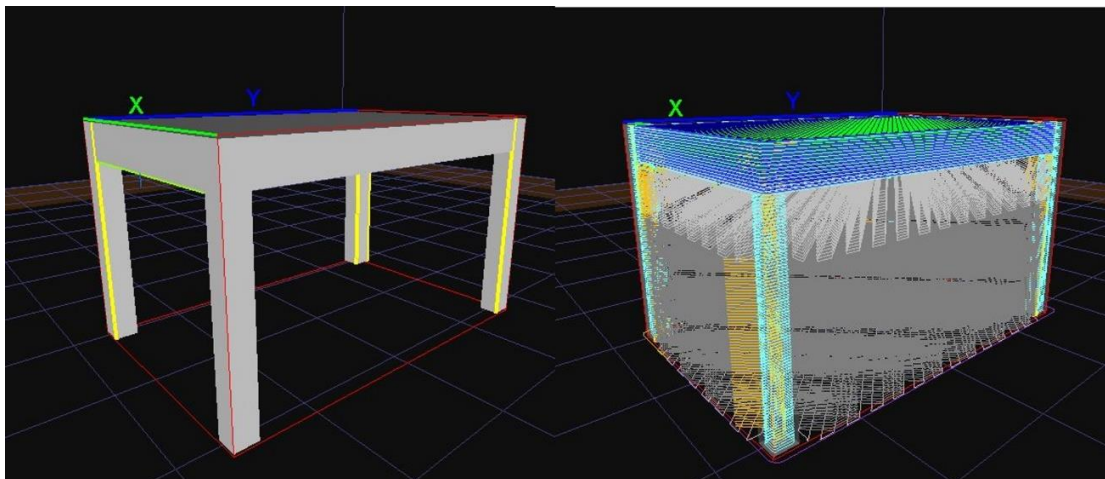
Figure 3.2-1 table posture 1 (estimated build time: 43.38 minutes)

34
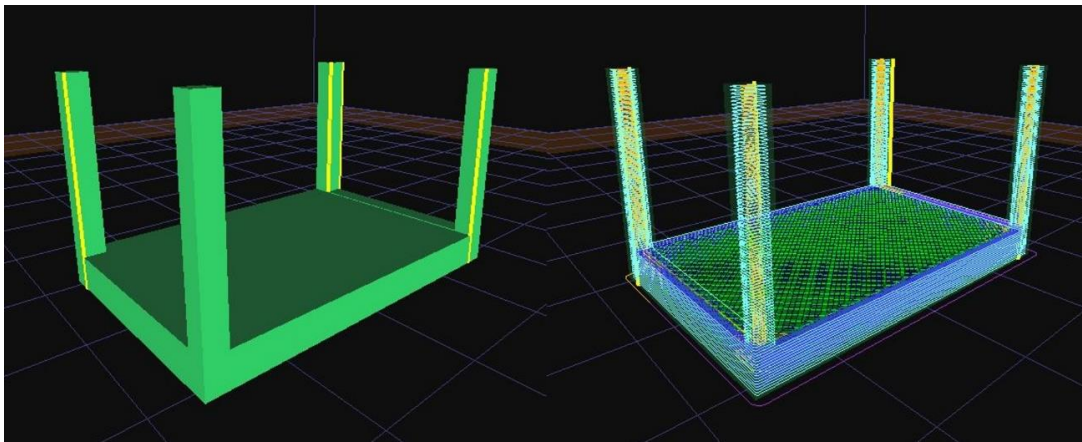
Figure 3.2-2 table posture 2 (estimated build time: 30.95 minutes)

3.3 Collision Consideration

After the models are obtained, we talk about how to avoid colliding with the printed parts. There are two steps in this section. One is that the bounding box of each model is determined. Second, combining bounding box with the hardware information calculates the collision region for each model. The two steps are described in details as follows.

- Generate the bounding box for each model

After we get the model in the proper posture, we can flatten the model to the XY plane to obtain the 2D maximum contour (see Figure 3.3-1). In other words, the 2D contour of top view of model can also be represented. However, the 2D contours are usually irregular. The irregular contours are difficult to be applied to the following steps (e.g. 2D Packing Algorithm). The computational complexity of the algorithm is very high, and it means that the computer needs to pay the high cost on the time consumption and computational resource, but the results are not outstanding compared with approximate method.

35
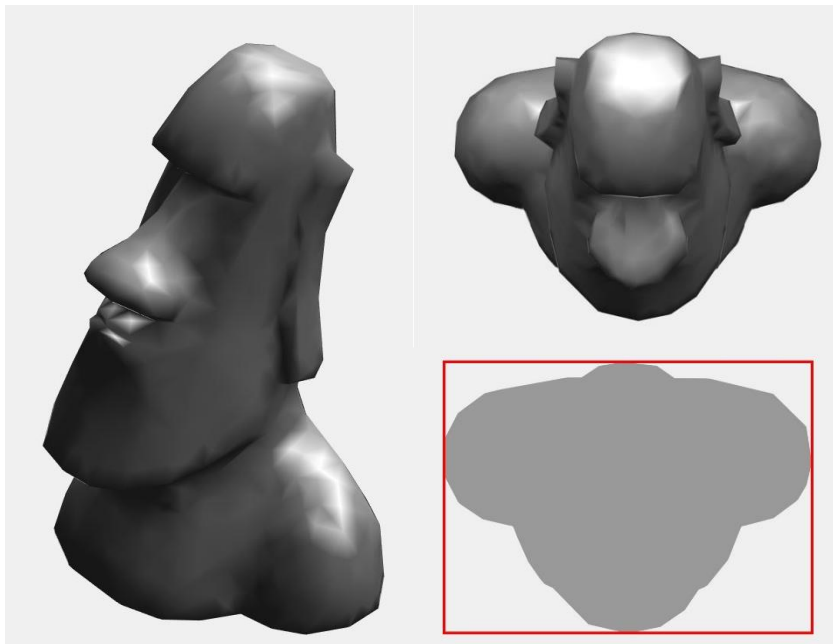
Figure 3.3-1 the left image is Moai model. Top right is the top view of the Moai model and lower right is the irregular contour.

Therefore, the bounding rectangle is used to approximate the irregular contour (see Figure 3.3-1). This approximate method not only makes the problem simpler but also significantly reduces the computational complexity of the algorithm. In Figure 3.3-1, the red color rectangle without rotating is called original bounding rectangle. The size of the original bounding rectangle may not be minimal. Therefore, we hope to calculate and obtain the minimum bounding rectangle to save printing workspace.

After that, we explain how to obtain the minimum bounding rectangle by seven steps as follows.

1. Compute convex hull of the object, then get a polygon.

2. Find all four extreme points for the polygon. Compute the area of the rectangle determined by the four lines, and keep as minimum.

3. Rotate the lines clockwise until one of them coincides with an edge of its polygon.

36
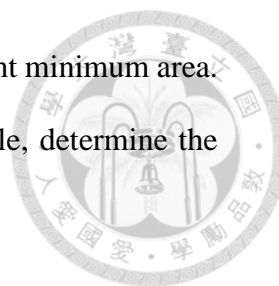
4. Compute the area of the new rectangle, and compare it to the current minimum area.

5. Update the minimum if necessary, and keep track of the rectangle, determine the minimum.

6. Repeat steps 3 - 5 until all edges have been processed.

7. Output the minimum area enclosing rectangle.

The result that is shown in Figure 3.3-2 displays that the shape of object is surrounded by two rectangles. The red rectangle is original bounding rectangle and its area is equal to $588.816\ cm^2$, while the area of green rectangle equals to $529\ cm^2$. Therefore, the green rectangle is called as the minimum bounding rectangle (MBR).
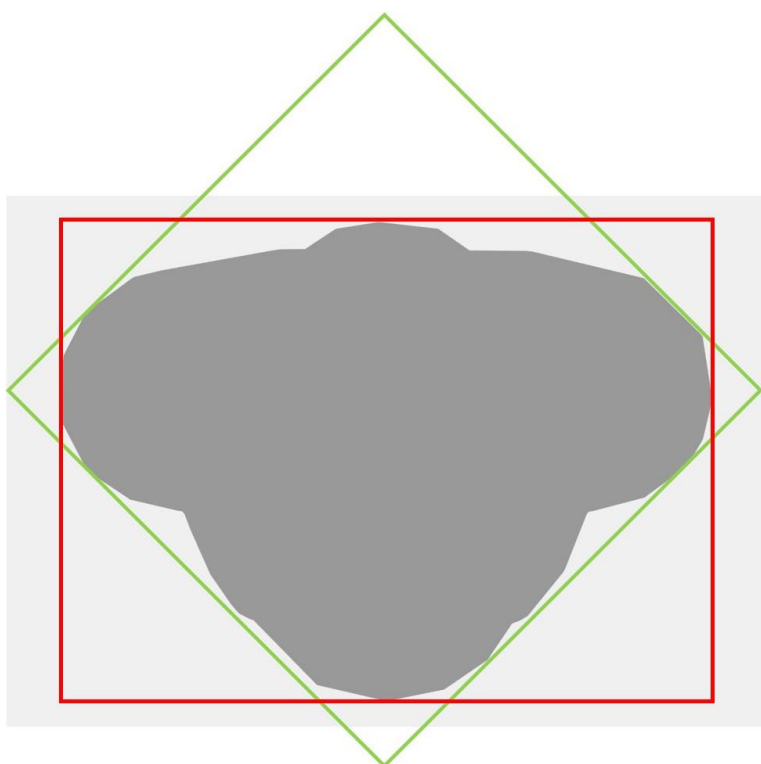
Figure 3.3-2 red rectangle is original bounding rectangle (Area : $588.816\ cm^2$), and green is minimum bounding rectangle (Area : $529\ cm^2$)

● Calculate the collision region

The collision region is inferred from hardware information. If the nozzle moves

37
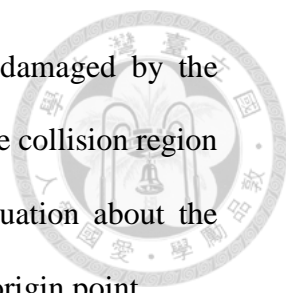
into the collision region, the printed parts may be collided and damaged by the extrusion nozzle. Therefore, how to decide the size and position of the collision region is an important issue in the printing process. We decide three situation about the collision region in Figure 3.3-3. And the nozzle tip is defined as the origin point.

Situation 1: the region is in the red dashed rectangle. It is close to the nozzle, we can express as Equation (3-1).

$$l_l < x < l_r, \qquad -\frac{n_d}{2} < y < \frac{n_d}{2} \qquad\qquad (3\text{-}1)$$

Situation 2: the region that is in the blue dashed rectangle excluding the area of the red rectangle can be represented as the Equation (3-2).

$$p_l < x < l_l \; or \; l_r < x < p_r, \qquad \frac{n_d}{2} > y > -\frac{n_d}{2} \qquad\qquad (3\text{-}2)$$

Situation 3: the area is other region which is not in red and blue dashed rectangle, and the conditions can be described as the following inequality.

$$x < p_l \; or \; x > p_r, \qquad \frac{n_d}{2} < |y| \qquad\qquad (3\text{-}3)$$
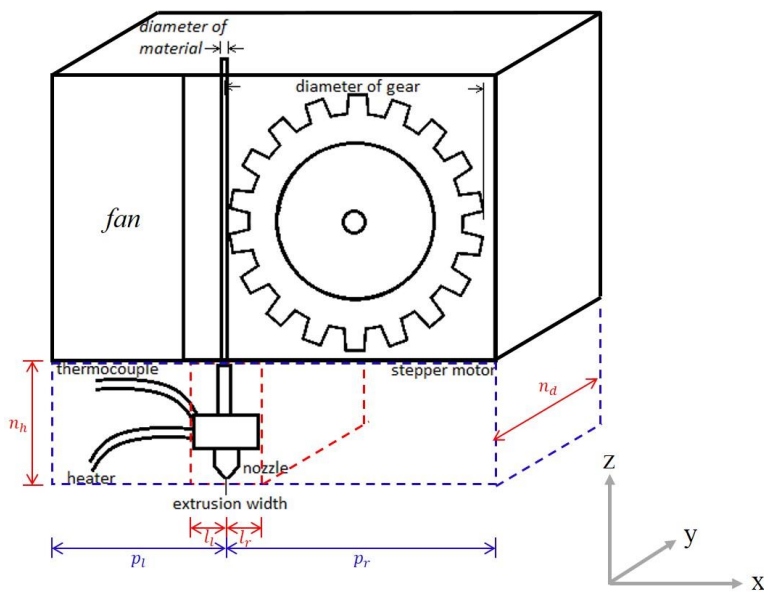
Figure 3.3-3 The illustration about collision region definition

38

After the minimum bounding rectangle of models are obtained, these rectangles are modified by collision conditions. In other words, expanding the rectangles are equal to increasing the safety distance between the printed parts and the nozzle in the printing process. We can determine the size of bounding box with collision conditions by using the relationship of relative motion between the nozzle and the printed model. In Figure 3.3-4, the dark gray area is maximum contour of model. The red, blue and gray rectangle are corresponded to situation 1, 2 and 3 respectively. Finally, the collision regions are defined and calculated simply. In order to clearly explain later, the ith collision region is defined as $R_i = (x, y, w, h)$, where (x, y) is the coordinate of the center of the rectangle and w and h are the width and height of the rectangle respectively.
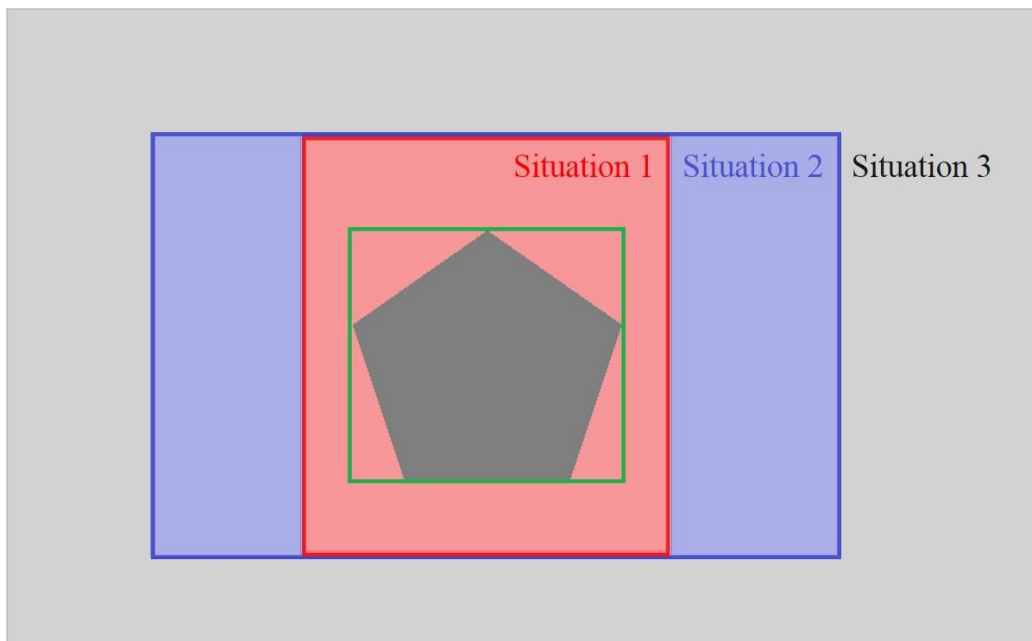
Figure 3.3-4 the dark gray area is maximum contour of model, and the green is minimum bounding rectangle. The red, blue and gray rectangle are corresponded to situation 1, 2 and 3 respectively.

39

3.4 Printing Strategy Evaluation

This step is how to choose the proper printing strategy for multiple objects according to the relationship between the size of workspace and area of collision regions. The size of workspace is decided as the set of points that can be reached by end-effector of machine, and the three collision regions that are mentioned above have been obtained. Our objective is to reduce production time and increase fabrication efficiency. The key is "transition travel" where the nozzle moves along among the objects without printing (show red color in Figure 3.4-1). Proposed algorithm attempts to minimize the transition travel distance as well as to improve motion path. Not only is some energy saved, but also the total manufacturing time is reduced directly.

As a result, we can sum up three strategies by using information about the size of workspace and collision regions. Three cases are described in detail as follows.
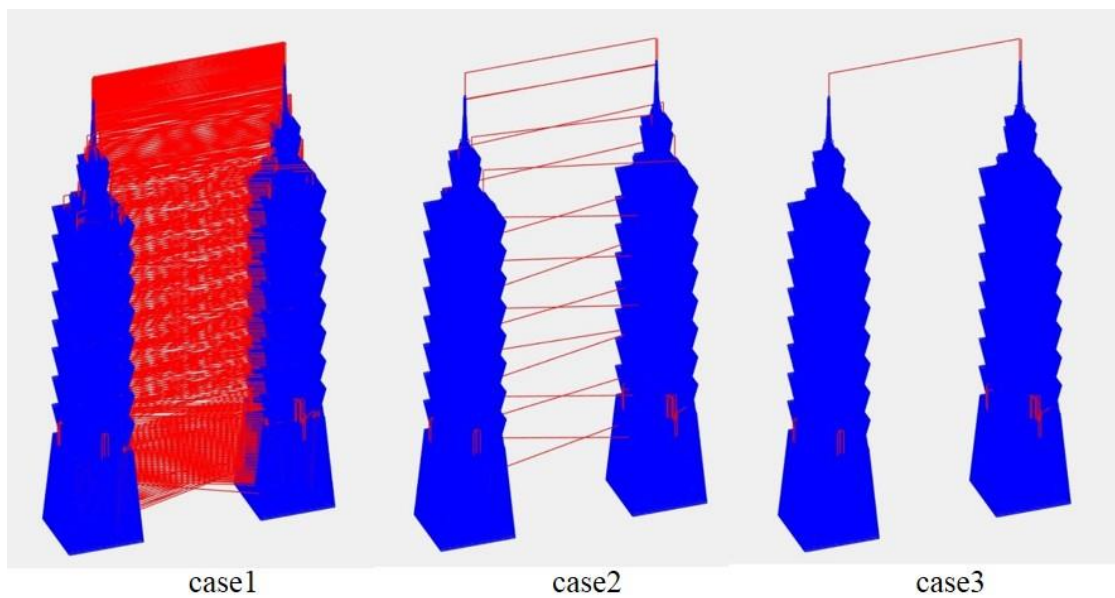
Figure 3.4-1 the blue line represents the printing paths and the red line is transition paths.

40
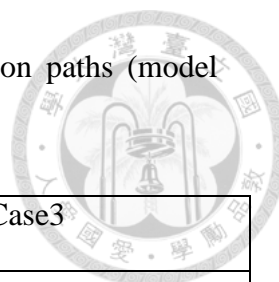
Table 10 the production time analysis on the printing and transition paths (model information: height is 100mm, number of layers is 392)

	Case1	Case2	Case3
Printing time(min)	94.64 (72.89%)	94.64 (98.83%)	94.64 (99.62%)
Transition time(min)	35.198 (27.11%)	1.1216 (1.17%)	0.3582 (0.38%)
Total time(min)	129.838	95.7616	94.9982

Case 1: print the models layer by layer.

The common slicing software uses layer by layer planning method to do printing path planning for multiple objects. Therefore, when multiple objects are printed at the same time, the nozzle moves among objects and always increases enormous distance of the transition travel. We use two 101 models as an example in order to clearly analyze the results shown in Figure 3.4-1. In the printing process, the nozzle moves to the next model after the first layer of first model is completed. Then, the nozzle returns to first model again after the first layer of another model is also completed. The process is finished when the models are built up.

Case 2: print the models part by part.

Optimizing the printing strategy reduces a lot of transition paths to increase printing efficiency and save extra energy. Printing the two object shows the process as follows. At first, print the model until appropriate height and move to next one. The second step is to print some layers until proper height, then return the first step. The recursive processing

41

is interrupted when the objects are completed. Obviously, the number of transition path between two objects is far less than the common slicing methods.

Case 3: complete the models one by one.

The model can be completed then move to the next one until all models are built up. This method is the most efficient and fastest in the three strategies. It can not only reduce much production time but also save more energy. However, the condition is that the workspace needs to be large enough so that the nozzle does not hit other printed objects during the printing process. The case 3 of Figure 3.4-1 shows the a few transition paths compared with the case 1 or case 2.

Therefore, the printing strategy is determined by the size of workspace and the area of minimum bounding rectangles.
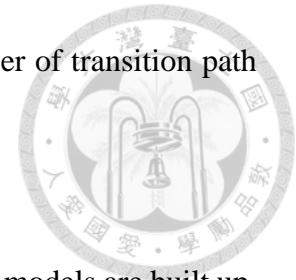
3.5 Planning Location of Multiple Objects

After the printing strategy is determined, the location of models are optimized to reduce the length of transition paths. We apply the 2D packing algorithm to arrange the collision regions to be optimized for placement. The 2D packing algorithm is based on genetic algorithm (GA), and the cost function of genetic algorithm is set as the sum of the distance among objects.

3.5.1   2D Packing Algorithm

The rectangular packing problem, also known as the two-dimensional (2D) packing problem, is a well-known combinatorial optimization problem which is the problem of orthogonally packing a given set of rectangles into a two-dimensional rectangular bin. Packing problems are concerned with finding a proper arrangement of multiple items in larger containing region. The objective of the allocation process is to minimize the cost function that is defined by ourselves.

The packing process has to ensure that there is no overlap between the items and no items can beyond the confine of workspace. These restrictions can be expressed as

$$A_i \cap A_j = \emptyset, i \neq j, \forall A_i, A_j, i = 1, \dots, n, j = 1, \dots, n \qquad (3\text{-}4)$$

and

$$A_i \cap A_w = A_i, \forall A_i, i = 1, \dots, n. \qquad (3\text{-}5)$$

where A_w is the area of the workspace, as well as A_i and A_j are the area of the collision regions. The number of collision regions is n.

Figure 3.5-1 shows the illustration of the packing problem, and the different

43

rectangles are represented as collision regions that are mentioned above. The block

rectangle is a workspace. After that, we use the genetic algorithm to solve the packing

problem.
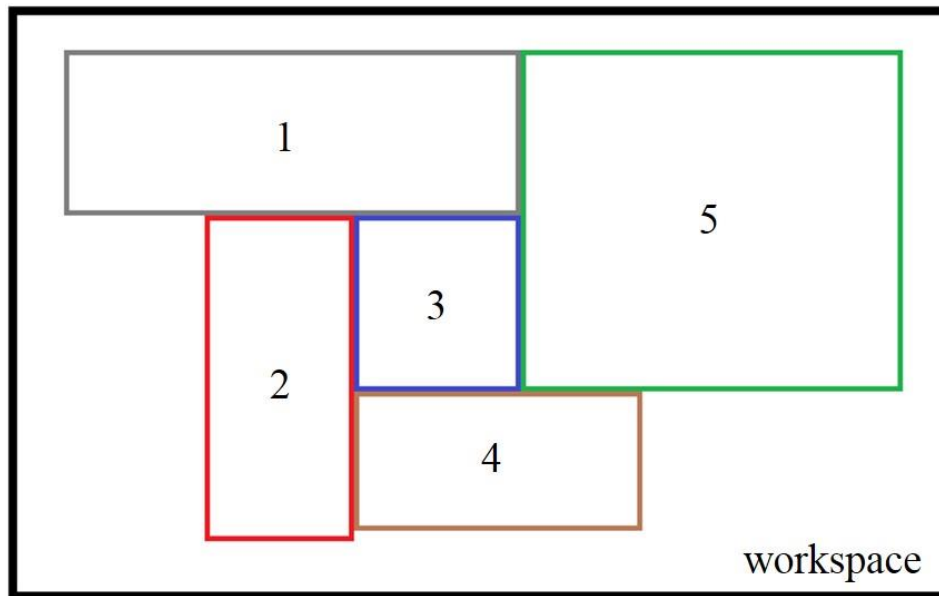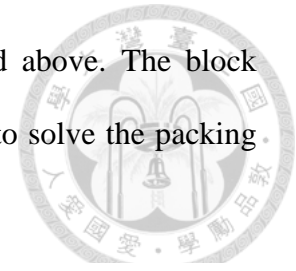
Figure 3.5-1 the illustration of two-dimensional packing problem.

3.5.2 Genetic Algorithm

Genetic algorithm (GA) is a metaheuristic inspired by the process of natural

selection that belongs to the larger class of evolutionary algorithms (EA). The main core

concept is natural selection and evolutionary processes. This algorithm is used to generate

high quality solutions to obtain the best solutions by relying on bio-inspired operators

such as selection, crossover and mutation. A population of candidate solutions, also called

individuals, chromosomes or phenotypes, is evolved toward better solutions through

multiple iterations. The evolution usually starts from a population of randomly generated

individuals, and is an iterative process, with the population in each iteration called a

44

generation. In each generation, the fitness, is usually the value of the objective function, as the indicator is evaluated to determine that every individual in the population is good or bad. The evolution indicator can be set as the value of the objective function or cost function, the two indicators are the opposite. Generally, the algorithm terminates when either the value of the cost function is lower than critical value for the population, or a maximum number of generations has been reached. Next, we talk about three bio-inspired operators in each generation.

● Selection

The selection is the stage of the genetic algorithm in which the individual genome is selected from the population for later reproduction. Fitness proportionate selection, also known as roulette wheel selection, is one of the most popular ways of parent selection. Every individual can become a parent with a probability which is proportional to its fitness. Therefore, the individuals with better fitness has a higher change of passing their features to the next generation.

No.	fitness	% of total
A	0.15	5
B	0.6	20
C	0.45	15
D	0.3	10
E	1.5	50
Total	3	100
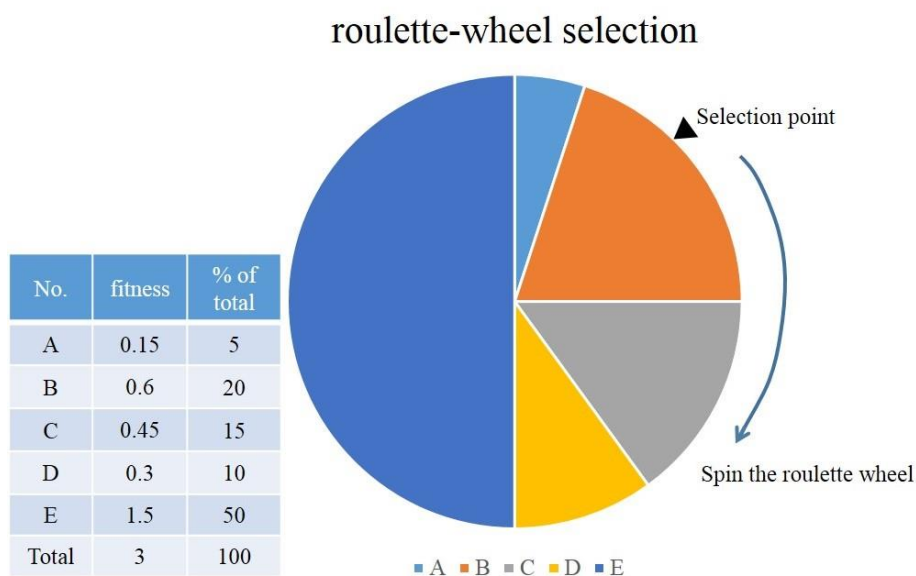
Figure 3.5-2 The illustration of the roulette wheel selection
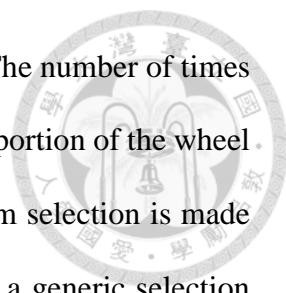
Figure 3.5-2 shows illustration of the roulette wheel selection. The number of times the roulette wheel is spun is equal to size of the population, and a proportion of the wheel is proportional to the fitness value of each individual. Then a random selection is made similar to how the roulette wheel is rotated. There are four steps in a generic selection procedure as follows.

◆ Step I. The fitness function is evaluated for each individual to obtain the fitness values, then the fitness value of each individual is divided by the sum of all fitness values to calculate the probability of each individual. Obtaining the probability process is called normalization, and we apply Equation (3-6) to describe it.

$$p_i = \frac{f_i}{\sum_{j=1}^{n_p} f_j} \times 100\% \tag{3-6}$$

where n_p is the number of individuals in the population. f_i is the fitness of individual i in the population and p_i is the corresponding probability of the fitness of individual i.

◆ Step II. The normalized fitness values are calculated and accumulated to become a cumulative probability that are shown in Figure 3.5-3 using Figure 3.5-2 as example.
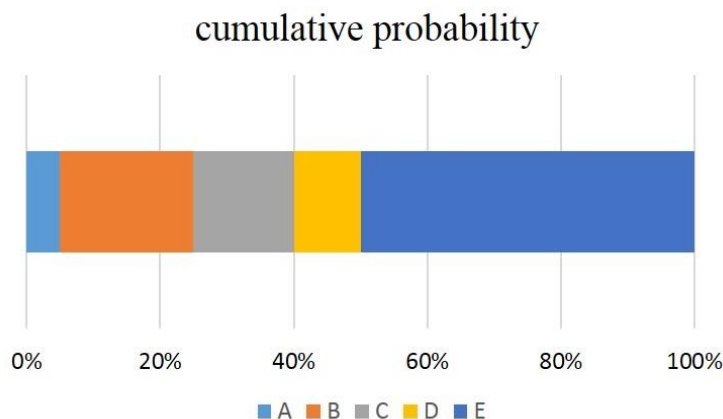
Figure 3.5-3 Cumulative probability
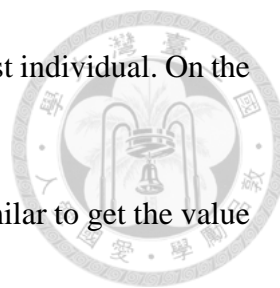
Figure 3.5-3 displays that the largest area indicates the fittest individual. On the contrary, the weakest individual has smallest area.

◆ Step III. Generate a random number R between 0 and 1. It is similar to get the value from the rotating roulette wheel.

◆ Step IV. The selected individual is the last one whose accumulated normalized value is smaller than R.

In the above description, we have the opportunity to choose not to excellent genes. Because not excellent genes may generate outstanding genes in next generation via genetic crossover or genetic mutation. As the natural selection process is based on performance indicators to choose individuals, and therefore the theoretical performance of the offspring should be higher than the parent. Finally, the approximate solution of the fitness function will be found during evolutionary process.

● Crossover

Crossover is a genetic evolution process that taking more than one parent solutions produces a child solution from them. In this section we will discuss how to modify crossover operator to be suitable for our case. Our case is to process the multiple rectangles arrangement and to obtain the optimal solution. Therefore, the information about a rectangle is stored as $R_i = (x, y, w, h)$ that is mentioned above, and the chromosomes can be seen as the (x, y). The w and h that are the width and height of the rectangle are decided by collision consideration process.

The chromosomes are picked out from the population by the selection process. Then whether the two chromosomes mate is determined by the crossover probability. If a random number is lower than the crossover probability, it means that the two chromosomes are going to do the crossover process. If not, the crossover process is

47
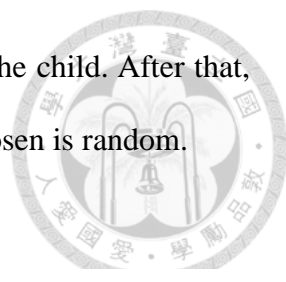
skipped and the chromosome of the parent is replicated directly to the child. After that, we design three cases in the crossover process, and which case is chosen is random.

Case 1:
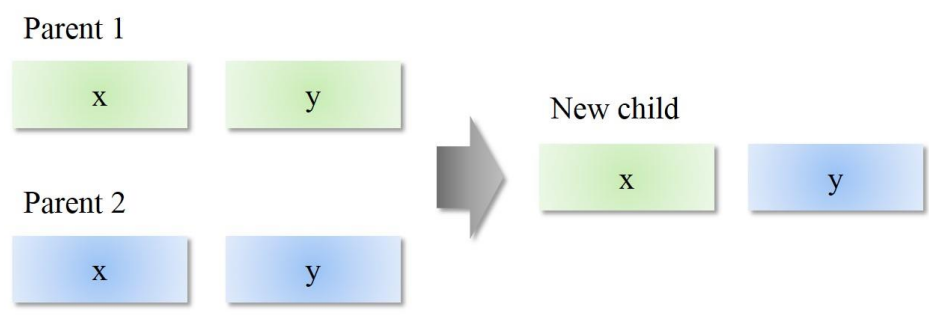
Figure 3.5-4 Case 1 selective crossover

Case 2:
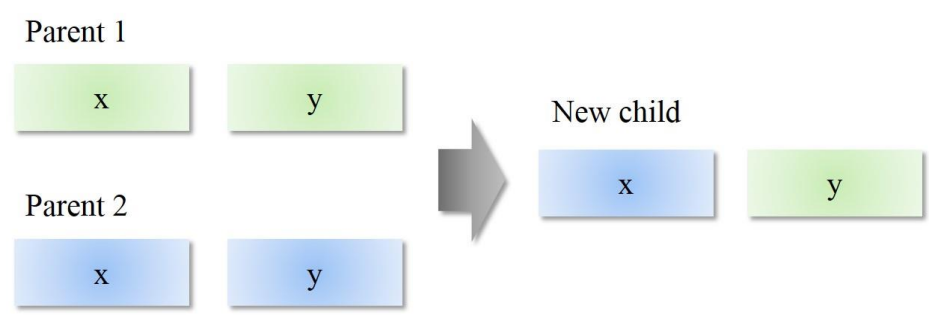
Figure 3.5-5 Case 2 selective crossover

Case 3:
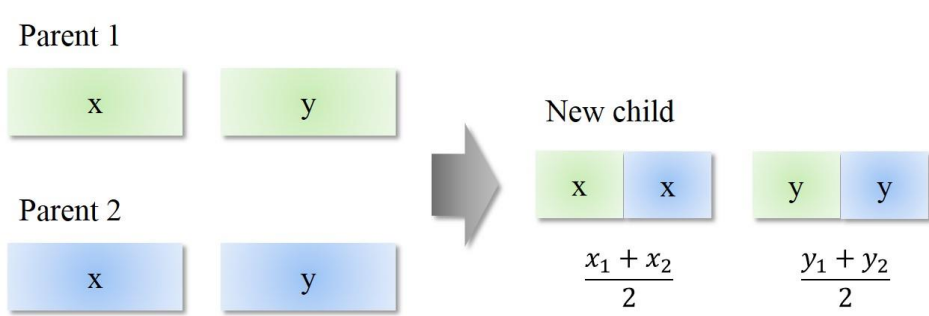
Figure 3.5-6 Case 3 crossover by using weighted average

The child in case 1 is generated by combining the x value of parent 1 with the y value of parent 2, and case 2 is similar to case 1. Case 3 uses the weighted average by two

48

parents to calculate the new child. The objective of crossover is to generate higher quality chromosomes by mating process.

- Mutation

Mutation, that is one of the evolutionary processes, can maintain genetic diversity from one generation of a population of genetic algorithm chromosomes to the next. The mutation process can avoid premature convergence of genetic algorithms, and solve the problems that the search space cannot be effectively searched and the solution falls into the local optimum. Mutation occurs during evolution according to a user-definable mutation probability. This probability should usually be set low. If it is set too high, the search will turn into a primitive random search. In our case, the x and y value of coordinate add the random values R_x and R_y respectively, and we can describe as follows.

$$(x, y) + (R_x, R_y) = (x + R_x, y + R_y) \tag{3-7}$$

Where the ranges of R_x and R_y are set as $-|w_w| + w < R_x < w_w - w \ and -|h_w| + h < R_y < h_w - h$ respectively. The w and h are width and height of the rectangle respectively and the w_w and h_w represent the width and height of the workspace.

The ranges of the random values R_x and R_y are determined by the size of the workspace and the size of the rectangle.

3.5.3 Cost Function Definition

The evaluation function commonly used can be distinguished into two types. On the one hand, cost function, also called loss function, is a function that quantifies an event or

49

status by mapping the one or more variables onto a real number. The value intuitively represents some "cost" associated with the event or status. On the other hand, an objective function, also known fitness function, indicates how much each variable contributes to the value to be optimized in the problem. An optimization problem seeks to minimize a cost function to obtain the optimal solution, while an objective function is either a loss function or its negative, in which case it is to be maximized.

Next, we design a cost function that corresponds to our problem. In our system, the distance among rectangles is shortened as much as possible. Therefore, the travelling salesman problem (TSP) is applied to our problem to generate the shortest possible route that visits each rectangle exactly once. The TSP model is written as follows, and label the center points of rectangles with the numbers $1, \cdots, n$ and define below.

$$x_{ij} = \begin{cases} 1, & the\ path\ goes\ from\ point\ i\ to\ point\ j \\ 0, & otherwise \end{cases}, for\ i = 1, \cdots, n \qquad (3\text{-}8)$$

Cost function:

$$min \sum_{i=1}^{n} \sum_{j=1, j \neq i}^{n} d_{ij}\, x_{ij} \qquad (3\text{-}9)$$

subject to

$$0 \leq x_{ij} \leq 1, for\ i, j = 1, \cdots, n \qquad (3\text{-}10)$$

$$u_i \in \mathbf{Z}, for\ i = 1, \cdots, n \qquad (3\text{-}11)$$

$$\sum_{i=1, i \neq j}^{n} x_{ij} = 1, for\ j = 1, \cdots, n \qquad (3\text{-}12)$$

$$\sum_{j=1, j \neq i}^{n} x_{ij} = 1, for\ i = 1, \cdots, n \qquad (3\text{-}13)$$

$$u_i - u_j + nx_{ij} \leq n - 1, for\ i, j = 1, \cdots, n \qquad (3\text{-}14)$$

where d_{ij} is the distance from point i to point j, and d_{ij} should be greater than or equal to zero and cannot be equal to infinity. u_i, a dummy variable, is an element of the set of integers.

Equation (3-12) requires that each city be arrived at from exactly one other city, and Equation (3-13) requires that from each city there is a departure to exactly one other city. The last constraints enforce that there is only a single tour covering all cities, and not two or more disjointed tours that only collectively cover all cities. If there are only two Equations (3-12) and (3-13), the situation that the sub-loop among the points cannot avoid may happen. Therefore, Equation (3-14) can avoid the formation of sub-loop.

When the shortest possible route are obtained, the distance that can be also calculated is a value of cost function. We use the value to evaluate the chromosomes in genetic algorithm.

3.6 Printing Procedure Optimization

The objective of the manufacturing process for multiple models is to reduce the production time, let the process be more efficient. There are two points that can be improved in this optimization problem. One is that reduce the transition path, the other is that increase the velocity of the nozzle movement on the transition path.

3.6.1   Printing path Optimization

As the above mentioned, optimize the motion path to reduce the total path and save extra transition time. The transition motion is reduced through arranging the location of

51

models and selecting proper printing strategy. For example, Figure 3.4-1 shows the simulation results of printing and displays the two Taipei 101 models which are printed by the three methods. The condition of case3 is that the workspace needs to be large enough so that the nozzle does not hit other printed objects during the printing process. Therefore, we focus on case1 and case2 here. Compared with the slicing software (case1), the decrease of transition path in case2 is obvious. The results of case1 and case2 are that the same objects are produced, while there is a 34.0764 minutes time difference between these two cases. Therefore, simplifying the transition path makes additive manufacturing more efficient and reduces the period of fabrication.

3.6.2   Motion Velocity Control

On transitive path part, the nozzle moves to next printable point as fast as possible. In order to minimize the transition time, we utilize two cases, triangular velocity profile and trapezoidal velocity profile, to control the speed of the transition segments. The transition length determines that every segment belongs to which cases. On the one hand, the triangular velocity profile means that the length of the transition segment is so small that nozzle speed can't reach the maximal velocity in Figure 3.6-1 (e.g. $t_2 \sim t_3$ segment). On the other hand, the length is long enough that nozzle speed can reach the maximal velocity, the velocity-time plot appears as the trapezoidal shape (e.g. $t_4 \sim t_7$ segment).

The critical condition is when speed-up is equal to the maximal velocity in transition segment. The critical value C can be calculated to determine that the interval between two points on the transition path belongs to triangular or trapezoidal velocity profiles. Hence, the critical value C can be defined as

52
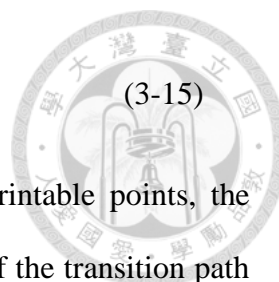
$$C = v_{motion} \cdot T + \frac{(v_{max} - v_{motion}) \cdot T}{2} \qquad (3\text{-}15)$$

where the distance of the transition path between the two printable points, the maximal velocity, and maximal acceleration are given. The length of the transition path be denoted as L, and maximal velocity and maximal acceleration are represented as V_{max} and A_{max} respectively. The definition of time T represents period during the triangular or trapezoidal velocity profile.

Using (3-15), the discriminant function value can be obtained. If $L \leq C$, absolutely it belongs to the triangular velocity profiles control. Otherwise, it belongs to the trapezoidal one. Assume the acceleration and deceleration are equal. The transition time of the velocity profile shows in Figure 3.6-1 can be obtained as follow:
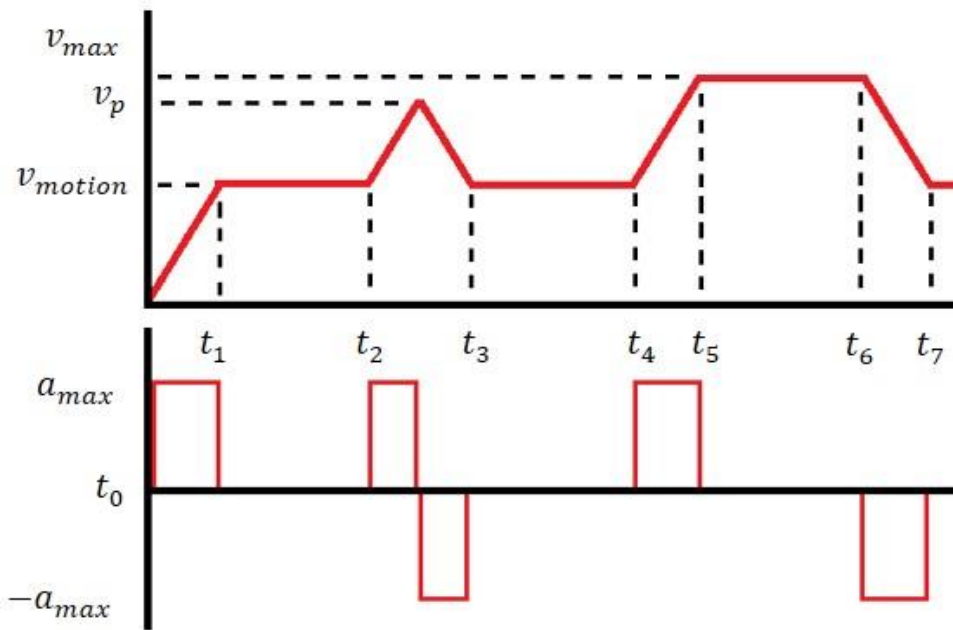
Figure 3.6-1 Velocity and acceleration profiles. On printing path segments $t_1{\sim}t_2$, $t_3{\sim}t_4$ and $t_7{\sim}$. On transition path segments $t_0{\sim}t_1$, $t_2{\sim}t_3$ and $t_4{\sim}t_7$.

Case1: transition time of triangular velocity profile (segment $t_2{\sim}t_3$)

$$v_p = \frac{T}{2} A_{max} + v_{motion} \tag{3-16}$$

$$\frac{T v_p}{2} + v_{motion} \cdot T = L \tag{3-17}$$

Using Equation (3-16) is substituted for (3-17), then we have

$$T = \frac{-6 v_{motion} + \sqrt{36 v_{motion}^2 - 4 A_{max} L}}{2 A_{max}} \tag{3-18}$$

Case2: transition time of trapezoidal velocity profile (segment $t_4 \sim t_7$)

$$L = v_{motion} \cdot T + \frac{(v_{max} - v_{motion})^2}{A_{max}}$$
$$+ (T - 2 \frac{v_{max} - v_{motion}}{A_{max}}) \cdot (v_{max} - v_{motion}) \tag{3-19}$$

Using (8), the transition time can be obtained as

$$T = \frac{L}{v_{max}} + \frac{(v_{max} - v_{motion})^2}{A_{max} v_{max}} \tag{3-20}$$

Equation (3-18) and Equation (3-19) show how to calculate the transition time. The printing speed of nozzle motion v_{motion} is given, so we increase the value of v_{max} and A_{max} under mechanical rating.

54

Chapter 4   Projection Algorithm based on Flattening Surface for Subtractive process

The objective of this paper is to describe the hybrid 3D printing approach to carving 2D image on the 3D curved surface based on surface flattening. Customized logo or trademark is supposed to be displayed on the surface of products, which cannot be completed only by 3D printing techniques. Projection algorithm, which transfers the 2D image to 3D sticker that matches the surface of products, is one of the techniques to satisfy this demand. In this paper, we propose a novel surface flattening algorithm that combines conformal mapping with optimal adjuster based on edge-lengths of the original mesh. By using the proposed algorithm, the surface of 3D model is unfolded. A two dimensional data or figure is mapped onto the unfolded plane. After the plane is mapped onto the 3D surface, a path for carving is obtained to sculpture the indicated figure onto the model. Moreover, compared with the several surface flattening methods, the proposed algorithm can minimize distortion while transferring 2D figure to 3D sticker. Furthermore, the algorithm is physically experimented on the gantry-type hybrid machine developed in our lab which integrates the additive (3D printing) and the subtractive (carving) process.

4.1 System Structure
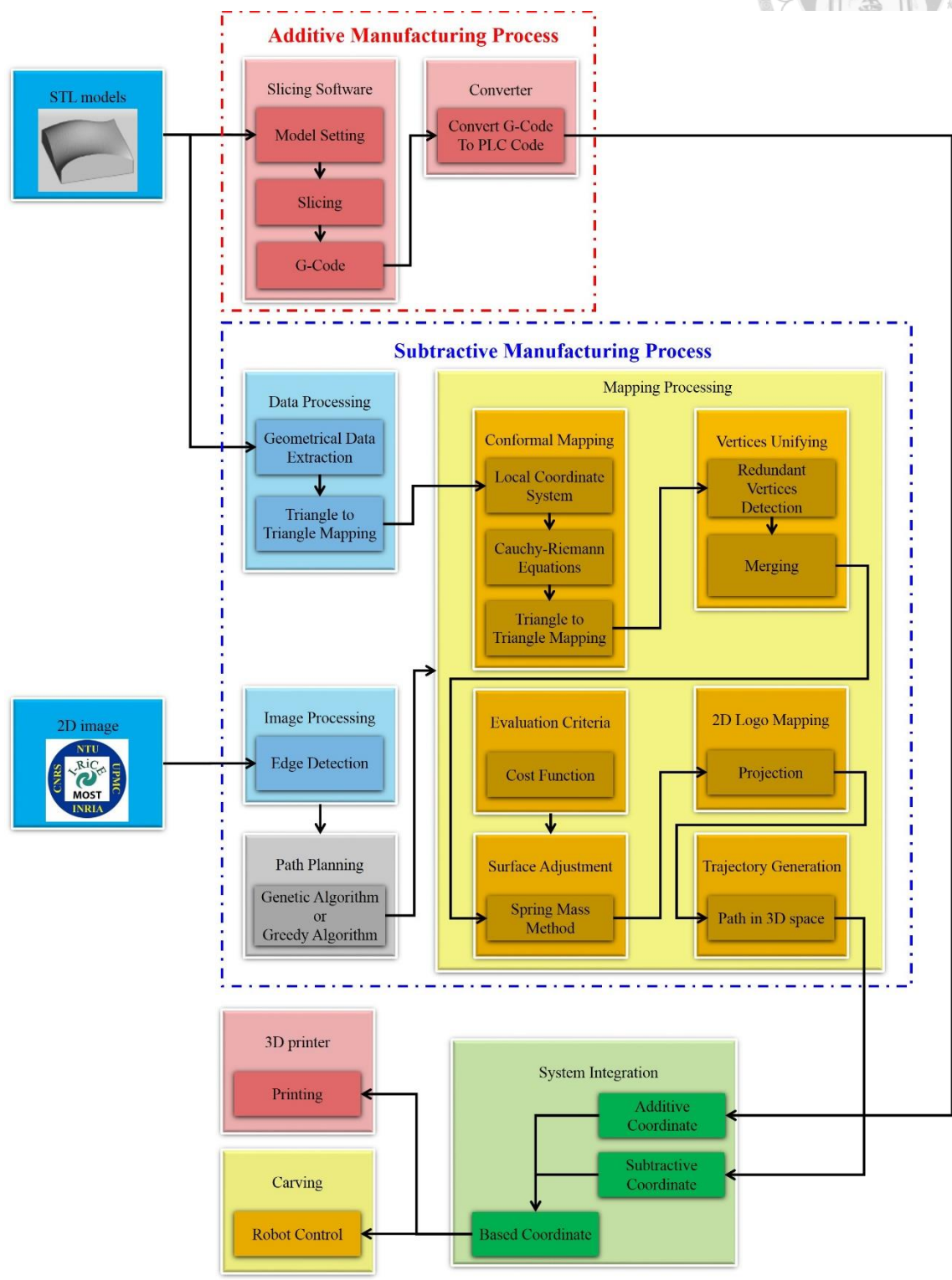
Figure 4.1-1 system flowchart

56

4.2 Projection Algorithm based on flattening method

The subtractive path for carving is obtained through the projection algorithm based on the surface flattening. The proposed algorithm focus on minimizing distortion and preserving the source data texture. The surface of the 3D model is expanded into 2D space, and the 2D logo or image can be intuitively projected onto the expanded plane by geometrical transformation. The projected flattening plane in 2D space can be reversely transformed into 3D space, where the reconstructed surface is fitted onto the original surface of the model, and get the motion information about end-effect position and rotation.

Our procedure for generating the carving path has five stages:

◆ Step I: The surface of 3D model is unfolded by using conformal mapping to obtain the expanded plane.

◆ Step II: If the vertex in the 3D mesh has more than one corresponding vertex in the 2D expanded plane, all of the vertices are merged into one point by weighted average.

◆ Step III: After that, we can get the approximate position for each vertex in the 2D expanded plane. Then, the vertices are adjusted to appropriate positions using edge-based flattening algorithm to minimize distortion of flattening plane.

◆ Step IV: The edge of the 2D data or logo can be extracted by using the image processing and be planned into the continuous path. Then, the continue path of the 2D data will be projected into the flattening plane.

◆ Step V: The projected plane in 2D space is mapped into the corresponding position of 3D model according to transformation matrix, and finally the carving trajectory in the 3D space is obtained.

As above steps are roughly described, then the details of every step are interpreted as follow.

4.2.1   Conformal mapping

The triangles on the surface of 3D model are transformed into the 2D plane, and it means $R^3 \rightarrow R^2$. Each triangle has the local coordinate system like Figure 4.2-1, and the triangle lies down on the x-y plane and z value is equal to zero. Therefore, the dimensions of coordinate transformation can be reduced to $R^2 \rightarrow R^2$. The complex system is convenient to describe the transformation relationship between the 2D spaces. The function f represents that the mapping relationship can transform this coordinate into the anther space. A geometric transformation $k = f(z)$ means that points in the x-y plane can be mapped onto points in the u-v plane and $z = x + iy$ and $k = u + iv$ are points in two different planes that are x-y plane and u-v plane respectively.
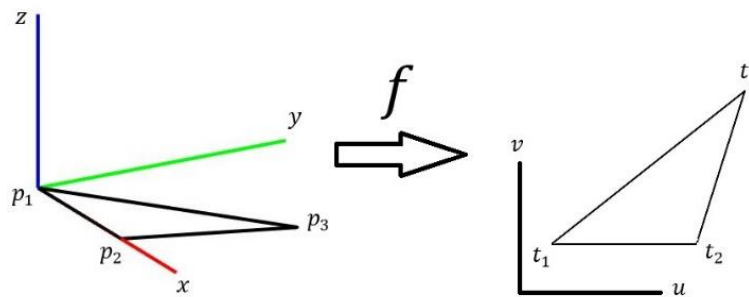
Figure 4.2-1 Triangle to triangle mapping

The surface of the 3D model is composed with of many triangular meshes to become a continuous closed surface. So, the transformation function $f(z)$ is conformal at any

58
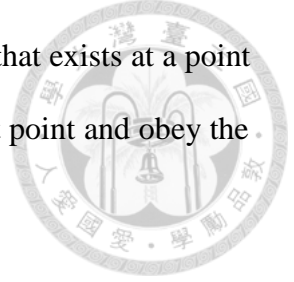
point where the derivative value is non-zero. The derivative of $f(z)$ that exists at a point z in x-y plane can infer the partial derivatives of u and v exist at that point and obey the Cauchy-Riemann conditions in Equation (4-1) and (4-2).

$$\frac{\partial u(x,y)}{\partial x} = \frac{\partial v(x,y)}{\partial y} \tag{4-1}$$

$$\frac{\partial u(x,y)}{\partial y} = -\frac{\partial v(x,y)}{\partial x} \tag{4-2}$$

Next, the local coordinate system of the triangles in the 3D space are calculated by geometry. Therefore, suppose that the X axis of local coordinate is the direction from p_1 to p_2 in the Figure 4.2-1. The information of the local coordinate including normal vector (Z axis) and Y axis is calculated by following Equations.

Suppose

$$\vec{X} = (p_2 - p_1)/|p_2 - p_1| \tag{4-3}$$

Then

$$\vec{N} = \vec{X} \times (p_3 - p_1)/|\vec{X} \times (p_3 - p_1)| \tag{4-4}$$

$$\vec{Y} = \vec{N} \times \vec{X} \tag{4-5}$$

The transform function f that vertices of the triangle $p_i(x_i, y_i)$ in the local coordinate transform to vertices of the triangle $t_i(u_i, v_i)$ in the u-v plane by affine transformation can be defined as follow.

$$f(z) = \frac{\triangle_{zp_2p_3}\, t_1 + \triangle_{p_1zp_3}\, t_2 + \triangle_{p_1p_2z}\, t_3}{\triangle_{p_1p_2p_3}} \tag{4-6}$$

where $\triangle$ is the area of the triangle and the subscript of $\triangle$ represents three vertices of the triangle. Therefore, the partial derivatives of f is calculated in Equations (4-7) and (4-8).

59

$$\frac{\partial f}{\partial x} = \frac{t_1(y_2 - y_3) + t_2(y_3 - y_1) + t_3(y_1 - y_2)}{2 \triangle_{p_1 p_2 p_3}} \quad (4\text{-}7)$$

$$\frac{\partial f}{\partial y} = \frac{t_1(x_2 - x_3) + t_2(x_3 - x_1) + t_3(x_1 - x_2)}{2 \triangle_{p_1 p_2 p_3}} \quad (4\text{-}8)$$

The above equations are utilized to calculate the Cauchy-Riemann equations, then we can obtain.

$$\frac{\partial u(x,y)}{\partial x} - \frac{\partial v(x,y)}{\partial y} =$$

$$\frac{1}{2 \triangle_{p_1 p_2 p_3}} (u_1(y_2 - y_3) + u_2(y_3 - y_1) + u_3(y_1 - y_2)$$

$$-v_1(x_2 - x_3) - v_2(x_3 - x_1) - v_3(x_1 - x_2)) = 0 \quad (4\text{-}9)$$

$$\frac{\partial u(x,y)}{\partial y} + \frac{\partial v(x,y)}{\partial x} =$$

$$\frac{1}{2 \triangle_{p_1 p_2 p_3}} (v_1(y_2 - y_3) + v_2(y_3 - y_1) + v_3(y_1 - y_2)$$

$$+u_1(x_2 - x_3) + u_2(x_3 - x_1) + u_3(x_1 - x_2)) = 0 \quad (4\text{-}10)$$

Solve Equations (4-9) and (4-10) to get the corresponding positions $t_i = (u_i, v_i), i = 1,2,3$, which are conformal on $f(x,y) \to (u,v)$. Each triangle can be converted into u-v plane by mapping function f. In order to get a unique solution for simultaneous equations, two vertices that contain four variables need to be fixed. Therefore, we need to decide the seed triangle, and one vertex of seed triangle is set as the origin of the u-v plane and another vertex of it is located on the u-axis. A triangle's edge which is formed by the two vertices that have been fixed on u-v plane can be transferred onto the u-v plane. For the other triangles, the triangle that satisfy the constraint that its two vertices have in the

flattening plane can be transferred onto the u-v plane. Finally, the flattening surface is obtained on the u-v plane.

4.2.2　Vertices unifying procedure in u-v plane

After a triangle to triangle transformation is obtain by mapping function $f(x, y) \rightarrow (u, v)$, the vertex in the 3D mesh has more than one corresponding vertex in the 2D expanded plane. In other words, the number of vertices in 2D plane is more than the number of vertices in 3D model. So, the redundant vertices that correspond to the same point in the 3D space are unified into one point by weighted average. The vertices unifying procedure is shown in Figure 4.2-2.

$$t_i(u, v) = \frac{\sum_{j=1}^{N_r} d_j(u, v)}{N_r} \tag{4-11}$$

where $t_i(u, v)$ is a vertex on u-v plane, and N_r and $d_i(u, v)$ are the number of redundant vertices and the redundant vertices that are transformed onto the u-v plane from the same point on the surface of 3D mesh. After that, we can get the stitched plane without overlapping or cracking.
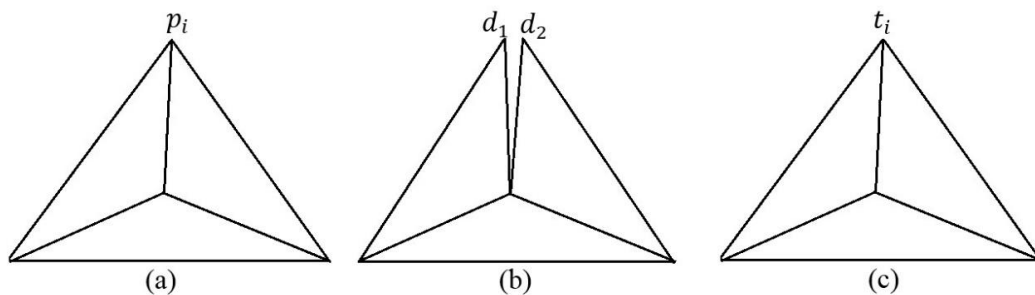

Figure 4.2-2 (a) the mesh of the 3D model. (b) the flattening surface by using conformal mapping (c) the vertices unifying procedure.

4.2.3　Adjust flattening surface

The step is in order to get an optimal flattening surface which has minimum error with the original surface, and the vertices in the 2D plane will be rearranged and adjusted to obtain the optimal mesh. Therefore, the cost function C that is the error between optimal mesh and original mesh is defined by edge-based flattening in Equation (4-12).

$$C = \sum_{i=1}^{N_e} w_{e_i}(L_i - l_i)^2 \tag{4-12}$$

where N_e is the number of edges on the surface mesh, and L_i and l_i are edge length of original mesh and optimal mesh. w_{e_i} is the weight factor of edge i

In the procedure, the conditions need to be satisfied to ensure that the surface mesh is feasible, and the conditions show as follow.

1.　Summation of angles around the vertex t_a is equal to 2π

Figure 4.2-3 shows that the summation of angles around the certain point equal to 2π, and this situation ensures that the faces around the point form the closed surface.

$$\alpha(t_a) = \sum_{i=1}^{N_a} a_i - 2\pi = 0 \tag{4-13}$$

$$for \ \forall t_a, a = 1,2,3, \dots N_v$$

The vectors of the edges that are known can calculate the angle a_i, and Equation (4-13) can rewrite as

$$\alpha(t_a) = \sum_{i=1}^{N_a} \arccos(\frac{\overrightarrow{e_a^{i-1}} \ \overrightarrow{e_a^i}}{\left|\overrightarrow{e_a^{i-1}}\right|\left|\overrightarrow{e_a^i}\right|}) - 2\pi = 0 \tag{4-14}$$

$$for \ \forall t_a, a = 1,2,3, \dots N_v$$

where N_a and N_v are the number of the angles around the vertex t_a and number

of the vertices, and a_i is the radian of the angle i. $\vec{e_a^i}$ is edge vector, of which the start

point is t_a , and $\vec{e_a^0} = \vec{e_a^{N_a}}$.
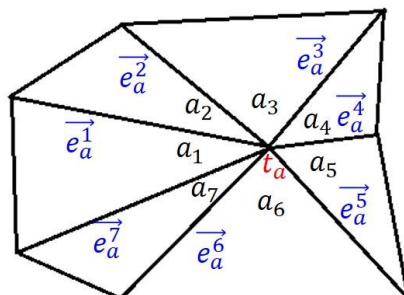
Figure 4.2-3 the edges and angles around the vertex t_a

2. The length must be positive

Each edge length is at least more than zero. The structure of triangle is destructed if

the edge length is equal to zero.

$$l_i > 0 \ for \ \forall l_i, i = 1,2,3, \dots N_l \tag{4-15}$$

The process not only needs to satisfy two constraints, but also minimizes the cost

function to obtain the optimal mesh. Using the spring mass method in Fig. 7 to calculate

proper location for each vertex. The stop condition of update process is that updated value

is smaller than ε.

$$t_i = t_i + \sum_{j=1}^{N_a} w_{e_i}(L_i - |\vec{t_i t_j}|)\vec{n_{ij}} \tag{4-16}$$

where N_a is the number of node connected to t_i, and $|\vec{t_i t_j}|$ is a distance between

the vertex t_i and vertex t_j on the flattening surface. And n_{ij} is the unit vector from

the vertex t_i to the vertices t_j that are connected with vertex t_i on the mesh. Before

the beginning of the process, we need to set up the seed point as the base point. Then

using the ripple-style flattening method to flatten the 3D surface. After all of vertices are

updated, the optimal mesh will be obtained.

4.2.4   2D logo is mapped into the flattening surface

This step is that the 2D data is projected onto the expanded plane. The raw data from 2D logo or image is preprocessed to extract the edges. The edges are composed of the many pixels and also can be represented as many points. However, the points are not sequential. Therefore, the points in 2D data are planned to become a continuous path by greedy algorithm or genetic algorithm. The points in the path are mapped into the flattening surface one-by-one.

4.2.5   Obtain the trajectory of the shape of logo in 3D space

After the above steps are completed, we can obtain the optimal flattening mesh. In this step, the target is obtaining the trajectory on the 3D model surface. Firstly, each point of path in the flattening surface finds the corresponding triangle, and the corresponding triangle on the 3D model can be inferred. Then, three lengths from the point to the three vertices of the triangle are calculated and normalize them to get the ratio that represents the relationship between the point and the three vertices. In corresponding triangle of the 3D model, after a point is mapping onto the 3D surface by using spring mass method, record the information about the position, normal vector of the triangle and the state of carving or not. Finally, the carving path is obtained when all of the points are transformed into the 3D space.
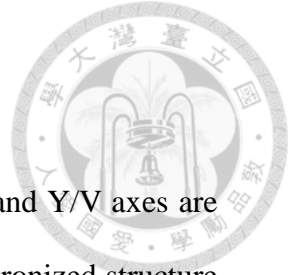
4.3 System Integration Process

In the gantry-type hybrid machine, the base axes including X and Y/V axes are composed of the linear motors, while Y and V gantry axes are synchronized structure which can improve the stability and accuracy of machine. The additive and subtractive parts share the X and Y/V axes while motions on vertical Z direction are individual. Therefore, our purpose is to combine the two parts together to print and carve on the same machine.

4.3.1   Additive Coordinate System

On the one hand, the 3D printer machine which has 3 degrees of freedom (DOF) can translate on 3D space. Equation (4-17) shows the transformation from system coordinate base point to the nozzle tip.

$$T^{base}_{nozzle} = \begin{bmatrix} 1 & 0 & 0 & linear\_axis\_X \\ 0 & 1 & 0 & linear\_axis\_Y \\ 0 & 0 & 1 & linear\_axis\_Z \\ 0 & 0 & 0 & 1 \end{bmatrix} \tag{4-17}$$

The path of the additive manufacturing is obtained by the slicing software and is transformed into the proper position by Equation (4-17). The nozzle head follows the transformed points and prints the material layer-by-layer on the table to build up the 3D model.

4.3.2   Subtractive Coordinate System

On the other hand, the subtractive part which has 5-DOF can translate and rotate on 3D workspace as well. Moreover, the gantry-type designed approach can decouple the

65

coordinate transformation into translation and rotation individually. This decouple designed method simplifies calculation and makes the transformation easier and clearer.

$$T_3^{base} = \begin{bmatrix} 1 & 0 & 0 & length\_axis\_X - linear\_axis\_X \\ 0 & 1 & 0 & linear\_axis\_Y \\ 0 & 0 & 1 & linear\_axis\_Z \\ 0 & 0 & 0 & 1 \end{bmatrix} \tag{4-18}$$

Equations (4-19) and (4-20) show the rotation matrix that rotates along the Z and Y axis respectively. The $\delta_{1\_x}, \delta_{1\_y}, \delta_{1\_z}, \delta_{2\_x}, \delta_{2\_y}$ and δ_{2_z} are set as zero because two rotary axes are perpendicular to each other. Equation (4-21) displays translation matrix that compensates the distance from common rotary center point to the tool tip.

$$T_4^3 = \begin{bmatrix} cos\theta_z & -sin\theta_z & 0 & \delta_{1\_x} \\ sin\theta_z & cos\theta_z & 0 & \delta_{1\_y} \\ 0 & 0 & 1 & \delta_{1\_z} \\ 0 & 0 & 0 & 1 \end{bmatrix} \tag{4-19}$$

$$T_5^4 = \begin{bmatrix} cos\theta_y & 0 & sin\theta_y & \delta_{2\_x} \\ 0 & 1 & 0 & \delta_{2\_y} \\ -sin\theta_y & 0 & cos\theta_y & \delta_{2\_z} \\ 0 & 0 & 0 & 1 \end{bmatrix} \tag{4-20}$$

$$T_5^3 = \begin{bmatrix} 1 & 0 & 0 & offset\_X \\ 0 & 1 & 0 & offset\_Y \\ 0 & 0 & 1 & offset\_Z \\ 0 & 0 & 0 & 1 \end{bmatrix} \tag{4-21}$$

Finally, the system coordinate base point can be transferred to tool tip by (4-22).

$$T_5^{base} = T_3^{base} + T_4^3 T_5^4 T_5^3 \tag{4-22}$$

In summary, the forward kinematics of the subtractive tool is obtained by Equation (4-22) so that the inverse kinematics can be calculated. The position and the direction of the carving tool are generated from the projection method, which will be transformed into base coordinate.

4.3.1 Coordinate Transformation

To simplify the procedure of customized fabrication, both additive and subtractive manufacturing are supposed to be integrated into a composite machine tool. On such composite machine tool, the additive process produces the 3D model from the STL data by fused deposition modeling (FDM) or fused filament fabrication (FFF). Then the subtractive part, with higher precision and flexibility, can do some more detailed processes like carving the customized logo and polishing the edge of the model to make it smoother. Nevertheless, there must be some error in size between the STL model and real product, which is resulted from the diameter of the nozzle head. This error may cause the problem that the tool tip misses the correct position. In other word, the tip may drill too deep into the surface of the model or even not touch the object.

To solve this problem, it is better to connect the path and position of subtractive part with those of the additive part. Since the additive and subtractive coordinates both can be transformed to base coordinate, it is easy to obtain the relationship between the nozzle head and tool tip. To compensate the error, this relationship can be used in the path planning of the subtractive manufacturing.

The system coordinate simulation is illustrated as shown in Figure 4.3-1. The left hand side is 3-DOF additive part and the other is 5-DOF subtractive part. There are some sub-coordinate systems in the figure. These sub- coordinate systems are represented as the frame of joints for each motor. The red, green and blue colors of sub-coordinate system are X, Y and Z directions respectively.
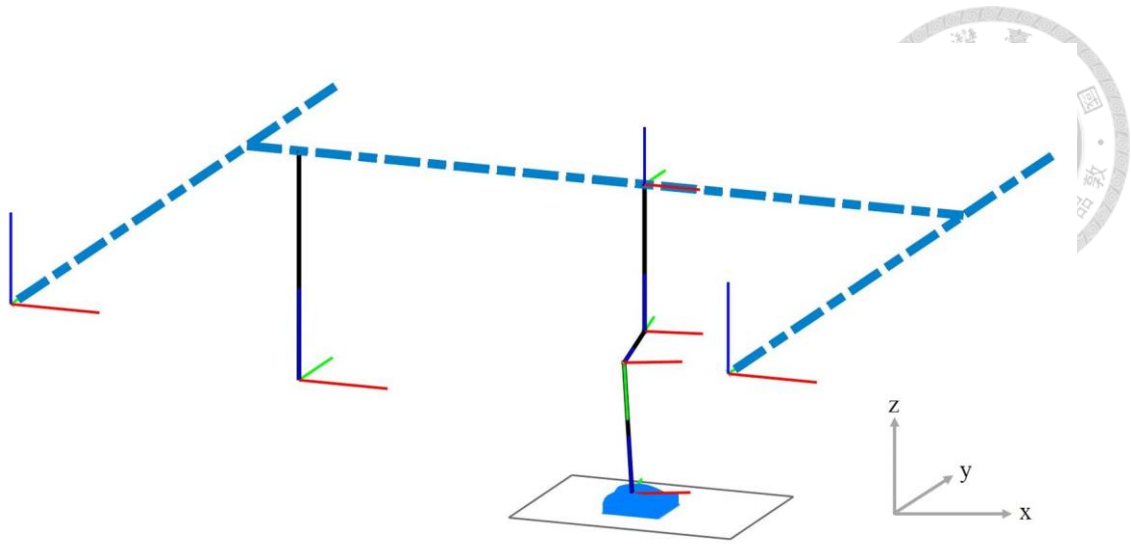
Figure 4.3-1 The illustration of the system coordinate simulation

Chapter 5　Experimental Results and Discussions

5.1 Multi-heterogeneous objects fabrication

5.1.1　Experimental Setup

In 3D printing industry, there is a significant technique about adjusting a balance between the machine velocity and extrusion speed. But if the machine velocity is faster than the corresponding extrusion speed, the melted thermoplastics cannot be deposited and even the material is snapped in two. On the contrary, if the machine velocity is slower than the corresponding extrusion speed, the unit area accumulates a huge mass of material and then the nozzle tip will also attach to the extruded material. Therefore, obtaining the relationship of nozzle velocity and extrusion speed is very important. We will talk about how to find the relationship between two speeds to let the 3D printing machine print normally.

The speed relationship is derived from the law of conservation of mass. In the law of conservation of mass, obtain the equation which the output mass is equal to the input mass as follows.

$$Mass_{input} = Mass_{output} \qquad (5\text{-}1)$$

Rewrite Equation (5-1) by using the equation of the mass,

$$V_{in}\rho_{in} = V_{out}\rho_{out}. \qquad (5\text{-}2)$$

where the volume of input/output are represented as V_{in} and V_{out} respectively. And ρ_{in} and ρ_{out} are density of input/output. The temperature of the input source is close to normal temperature and the material of input presents solid. However, while the

69

temperature of the output source is up to about 220 degrees in Celsius for PLA material and the material of output becomes to be gelatinous liquid. So when we calculate the density, the thermal coefficient of expansion needs to be considered. The values of ρ_{in} and ρ_{out} are equal to 1210 and 1430 kg/m^3 respectively.

In Figure 5.1-1, the diameter of the nozzle and material, and the diameter of the gear, and the density of input/output are given. For the next step, assume the speed of nozzle motion and angular velocity of the stepper motor are represented as v_{motion} and ω_{motor}, respectively. And we get Equation (5-3).

$$v_{motion} = \alpha \frac{D_{gear}}{2} \omega_{motor} \frac{D_{material}^2}{D_{nozzle}^2} \frac{\rho_{in}}{\rho_{out}} \qquad (5\text{-}3)$$

where α is a fine-tune parameter, and $\omega_{motor} = 2\pi \frac{F_{in}}{N}$, F_{in} and N are denoted as input pulses per second and amount of steps that will drive the motor to turn a full circle. The diameter of the gear of step motor, the diameter of material, and the extrusion width are denoted as $D_{gear}, D_{material}$ and D_{nozzle} respectively. Equation (5-3) means that the value of nozzle motion speed is calculated according to the speed of step motor. In another word, changing the speed of the step motor can adjust the speed of the nozzle automatically.

The α is fine-tune parameter and it can change the width of the deposition. In other words, if α is more than one, it means that the nozzle motion moves faster than normal. Therefore, the width of the deposition will be thin. The relationship of nozzle velocity and extrusion speed reflects in the quality of the results in Figure 1.4-2.
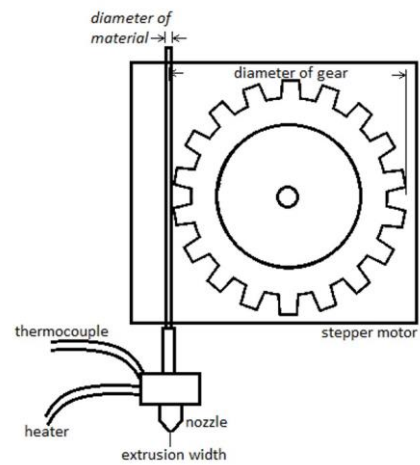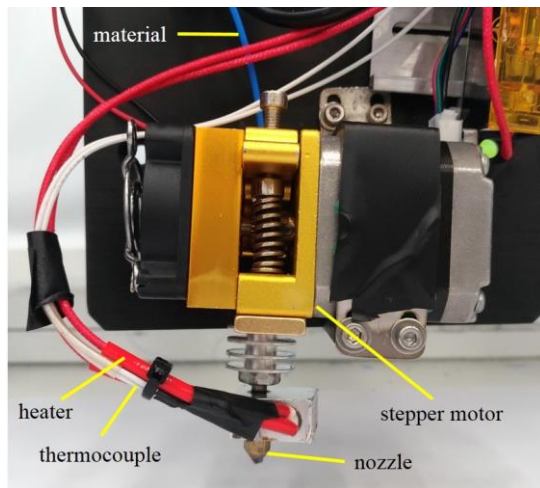
Figure 5.1-1 The extrusion system has some components including a nozzle, a stepper motor, a heater, a thermocouple, etc.
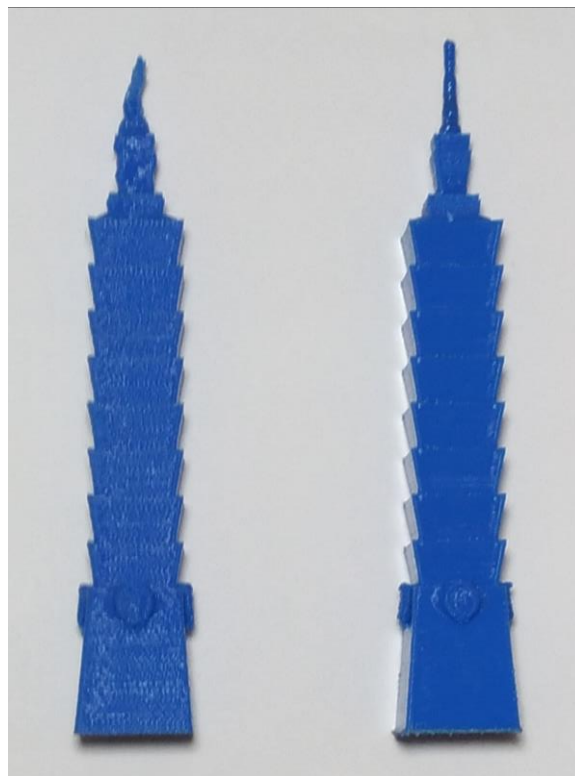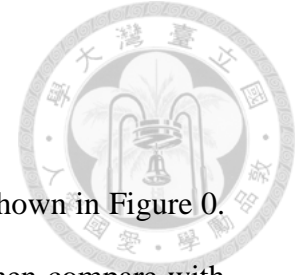

Figure 5.1-2 The relationship of nozzle velocity and extrusion speed reflects in the quality of the results.

71

5.1.2   Experimental Results

The results about multi-heterogeneous objects fabrication are shown in Figure 0. Firstly, we can analyze the estimated build time for each object. Then compare with the results that are generated by KISSlicer slicing software [27].
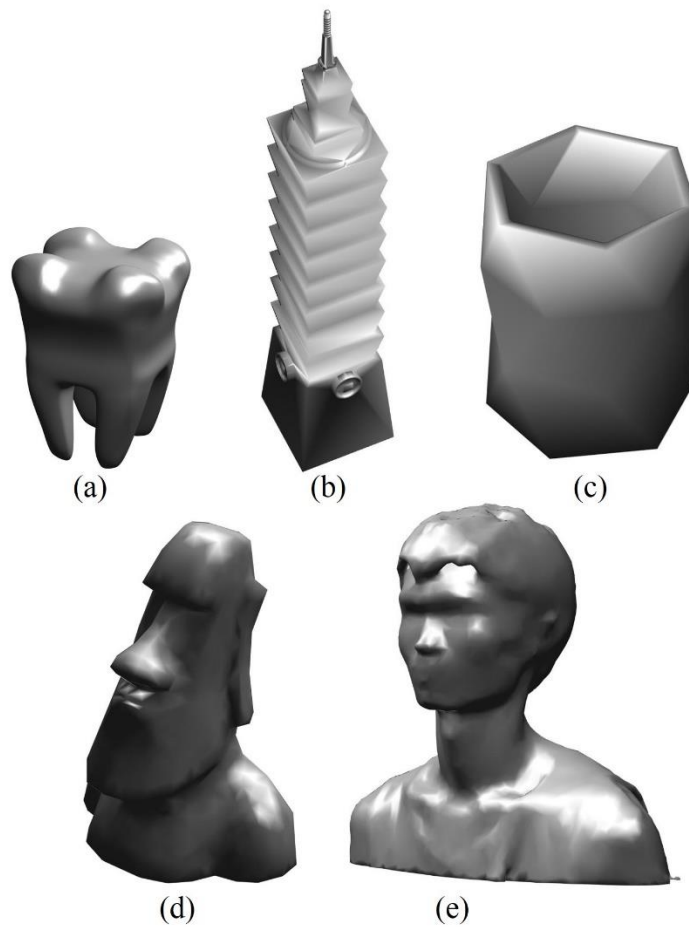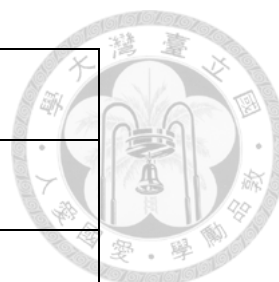
Figure 5.1-3 (a) tooth (b) Taipei 101 (c) pen holder (d) Moai (e) statue

Table 11 the building time for each object

	Building time
(a) tooth	53.47 minutes
(b) Taipei 101	156.21 minutes

(c) pen holder	196.15 minutes
(d) Moai	121.22 minutes
(e) statue	274.30 minutes

Setting parameters (layer thickness: 0.2mm, infill: 16.7%, extrusion width: 0.4mm)

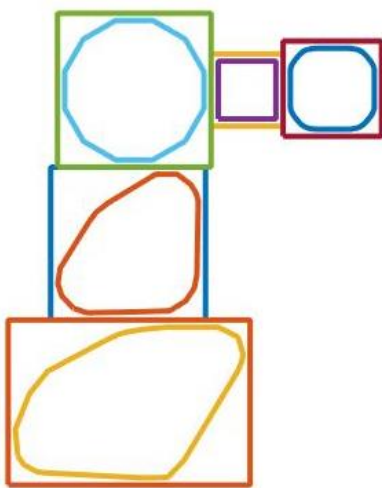Case 1: print the model layer by layer

Figure 5.1-4 Location of multiple objects with top view
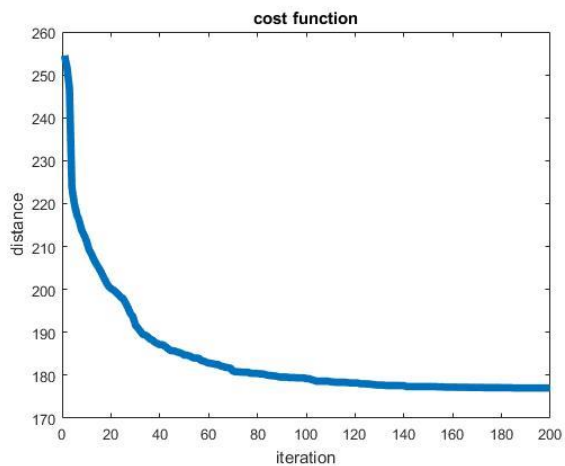
Figure 5.1-5 Cost function (best chromosomes in genetic algorithm)

Figure 5.1-6 Cost function (best chromosomes in genetic algorithm)

Case 2: print the model part by part

Figure 5.1-7 Location of multiple objects with top view

Figure 5.1-8 Cost function (best chromosomes in genetic algorithm)

Figure 5.1-9 The result by our proposed method. The blue line represents the printing path and the red line is transition path.

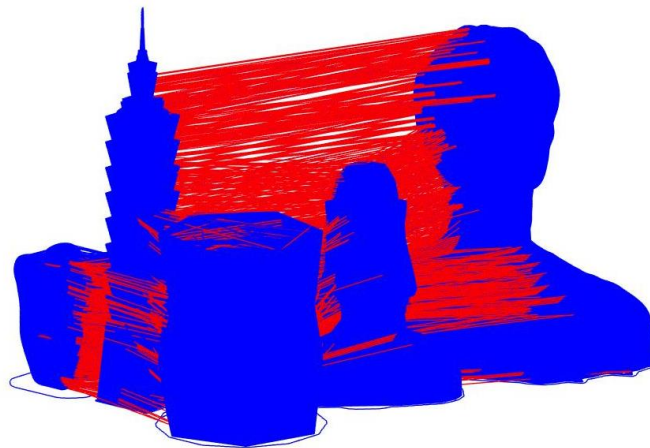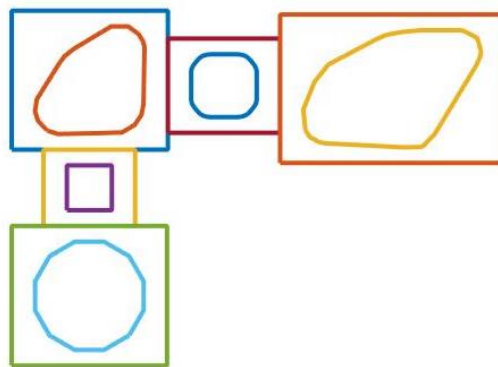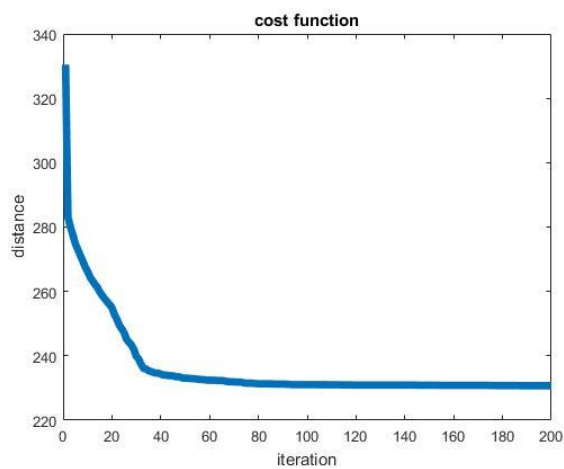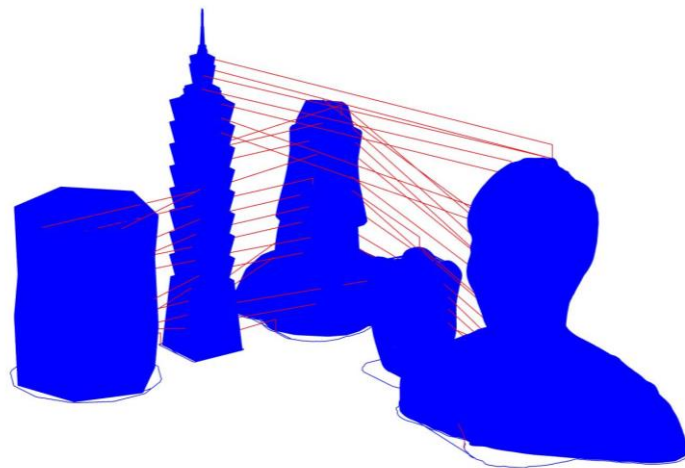Case 3: complete the model one by one (ideal)
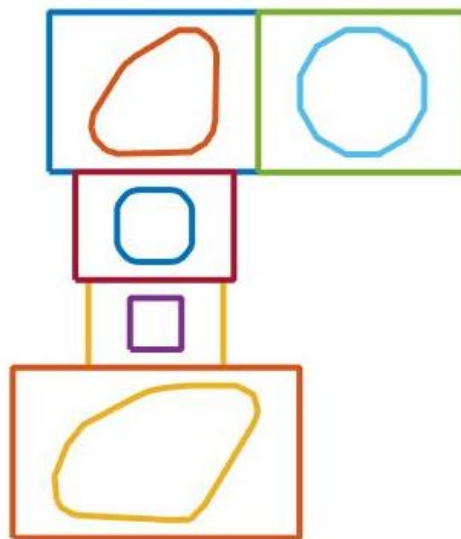
Figure 5.1-10 Location of multiple objects with top view

75
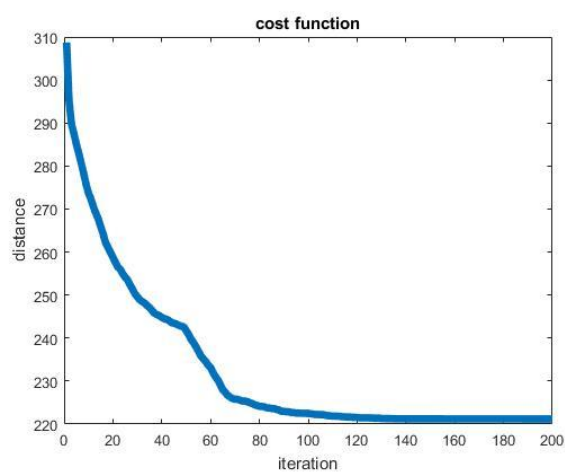
Figure 5.1-11 Cost function (best chromosomes in genetic algorithm)
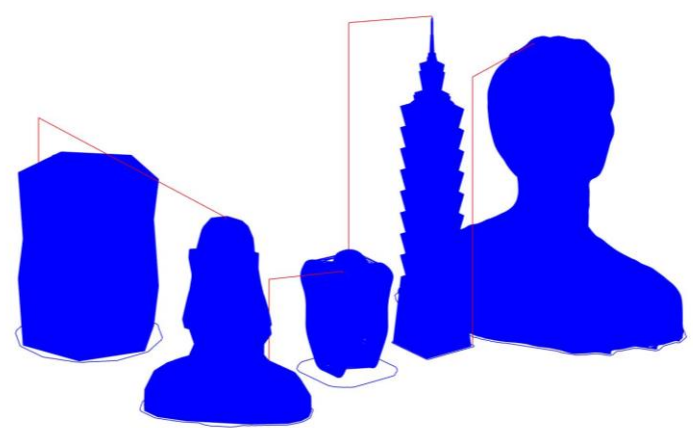
Figure 5.1-12 Ideal result of the printing

There are three printing strategies in our results. The printing path is labeled as blue color, and the transition path is represented as red color. The blue parts of the all cases represent our objects, and its path usually cannot be changed unless the model is replaced by other. The results of case 1 use the layer by layer printing method to build up the models. Therefore, the nozzle takes some time to move on the transition among objects. The transition path of case 2 that is our proposed method is less than case1 so that the production time is also less than case 2. The case 3 needs to have the large workspace so that the nozzle does not collide with the printed parts during the printing process, and we can observe that the bounding rectangles of case 3 are larger than case

76
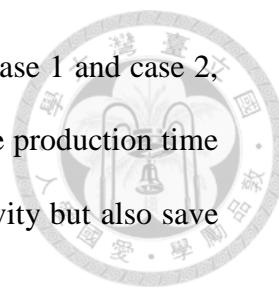
1 and case 2. Therefore, we will focus on the comparison between case 1 and case 2, and Table 12 shows the production time of the three strategies. If the production time is reduced in the industry, let the factory not only improve productivity but also save energy consuming.

Table 12 the production time of three strategies

	Printing time	Transition time	Total time
Case1	801.35min (90.26%)	86.5192min (9.74%)	887.8692 min
Case2 (proposed)	801.35min (98.51%)	12.1031min (1.49%)	813.4531 min
Case3(ideal)	801.35min (99.81%)	1.5333min (0.19%)	802.8833min

5.2 Projection algorithm based on flattening surface

In this section, we demonstrate the projection results by proposed projection algorithm based on flattening surface and compare with other projection method. The procedure of details on the projection algorithm are mentioned above.

5.2.1   Experimental Setup

In the experiment, the cooperation of the additive and subtractive manufacturing is implemented through inverse kinematics. In other words, the 3D printer and carving tool can be controlled precisely and be cooperated to complete the product. The specification

of gantry-type hybrid machine is explained that the length of the X and Y axes are 1.5m and 1.8m respectively. The height of additive and subtractive are 0.36m, and the tool tip offsets in X, Y and Z direction are 0, 100mm and 120mm respectively.

After that, the integration system with additive and subtractive manufacturing is demonstrated. 3D printer can print the model and the subtractive tool follows the position and direction that are obtained by proposed projection method. In the additive process, the 3D STL model is sliced to generate the moving path from the slicing software. One kind of materials called polylactic acid (PLA) is used as the printing material. The melting point of PLA is from 155 to 170 degrees centigrade.

As mentioned above, the path of the additive information is passed to the subtractive process as the reference data. The reference data and the coordinate of the subtractive tool are considered to adjust the carving path brought by the projection method. Three different kinds of tool tips (shown in Figure 5.2-1) are tested in our experiment.

The rotational speed of the subtractive tool is up to 12000 revolutions per minute (RPM). When the subtractive tool contacts the printed model, the temperature of the material rises quickly due to high speed friction. As we known, the PLA material becomes stickier with the rise of the temperature so that the extra material will attach to the drill probably (Figure 5.2-2).
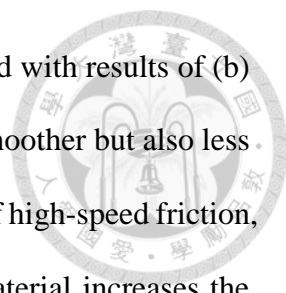
Figure 5.2-1 The three different carving tools. Left to right : (a) The cone drill. (b) The twist drill. (c) The round drill.

Figure 5.2-2 The tool tip after subtractive process.

The final results of the test using three kinds of drills are shown in Figure 5.2-3 in order. In this test, three same square sheets are printed by the additive part using PLA. And then the aforementioned drills are installed respectively to complete the subtractive process. All the drills are stuck into the sheets with the same depth during the test.

79

Obviously, the cone drill of Figure 5.2-1 (a) performs best. Compared with results of (b) and (c), the carving path in Figure 5.2-3 (a) is not only clearer and smoother but also less in the width. It is because no extra material, which is molted by heat of high-speed friction, attaches to the tip while doing subtractive process. The attached material increases the width of carving path so that it affects smoothness of the subtractive performance as well. This phenomenon is also seen in the result of the subtractive process with the twist drill shown in Figure 5.2-2 (b). The green point is the start point of the subtractive path that moves along the clockwise direction while the red point is the point where the width of the subtractive path starts to be enlarged. This point is also where the molted material starts to attach to the drill. And comparing the drill after subtractive processing and the results of (b) and (c), the width of path of the twist drill is narrower than that of the round drill while more extra material is stuck to the round drill than that of the twist drill. So it is verified that the more extra material attaches to the drill, the larger radium of the drill will be and the wider the subtractive path will be generated.
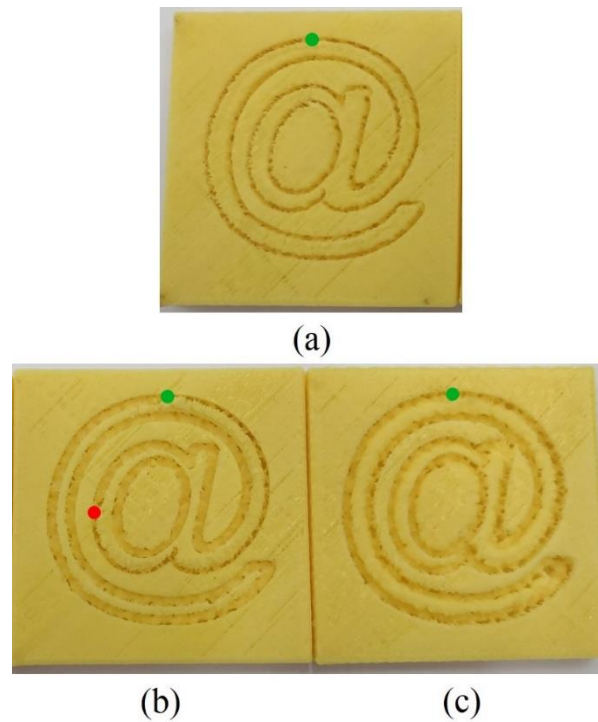
Figure 5.2-3 The carving results by using the different tools: Left to right: (a) The cone drill. (b) The twist drill. (c) The round drill.

5.2.2 Experimental Results

Figure 5.2-4 and Figure 5.2-5 show the surface models and flattening results, respectively. In the Table 13 and Table 14, compare with other flattening method that is angle based flattening (ABF). In the results of proposed method, the angle error is a little larger, but the edge length error and the area error is much less.

<div align="center">(a)   (b)</div>

Figure 5.2-4 (a) the triangular mesh of the 3D model. (b) flattening result. (hemisphere mesh data: number of vertex : 145; number of face : 264).

<div align="center">Table 13 Compare with typical methods on hemisphere surface</div>

	Length error	Angle error	Area error
EBF(proposed)	0.0885	0.11365	0.049692
ABF	0.13159	0.10302	0.097674

<div align="center">(a)   (b)</div>
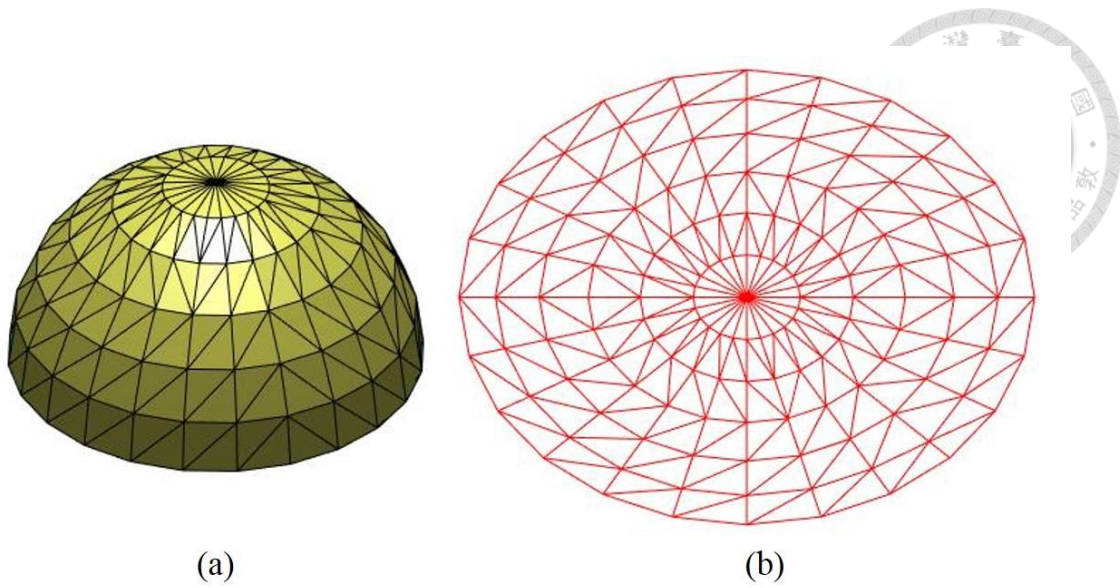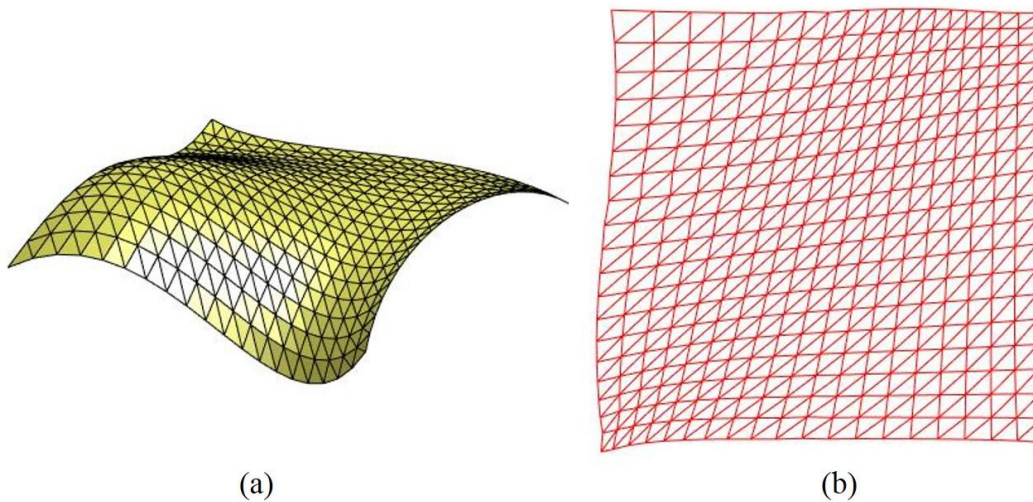
Figure 5.2-5 (a) the triangular mesh of the 3D model. (b) flattening result. (wave mesh data: number of vertex : 400; number of face : 722)

Table 14 Compare with typical methods on wave surface

	Length error	Angle error	Area error
EBF(proposed)	0.020367	0.037288	0.030595
ABF	0.028007	0.03127	0.065139

In the data processing, if the input data is the 2D image or figure, it is processed by image processing that contains the color transformation from RGB to gray level and edge detection. Afterwards, the points that are extracted from the edge image can be planned into a continue path using greedy algorithm or genetic algorithm. Then, as for the subtractive part, the tool can touch the corresponding triangles of top part on the model because of its 5-DOF. Thus, the available triangular flats on the STL model are reserved and filtered out the useless flats by determining whether the normal vector norm of the flat is more than zero or not. In other words, choose the flats (label yellow color in Fig. 2) that can be carved by the subtractive tool.

After the steps of data preprocessing, the processed data can be utilized in projection procedure. Fig 11 shows the result that how the 2D data is projected onto the geometric models. On the model, the data of each point on the projected path contains three components. The first is the coordinate of the point. The second is the carving signal that determines whether the point should be carved or not. The third component is the normal vector of the triangle where the point is inside. After that, it can be ensured that the machine moves to the correct coordinate and the subtractive tool is perpendicular to the surface of the 3D model.
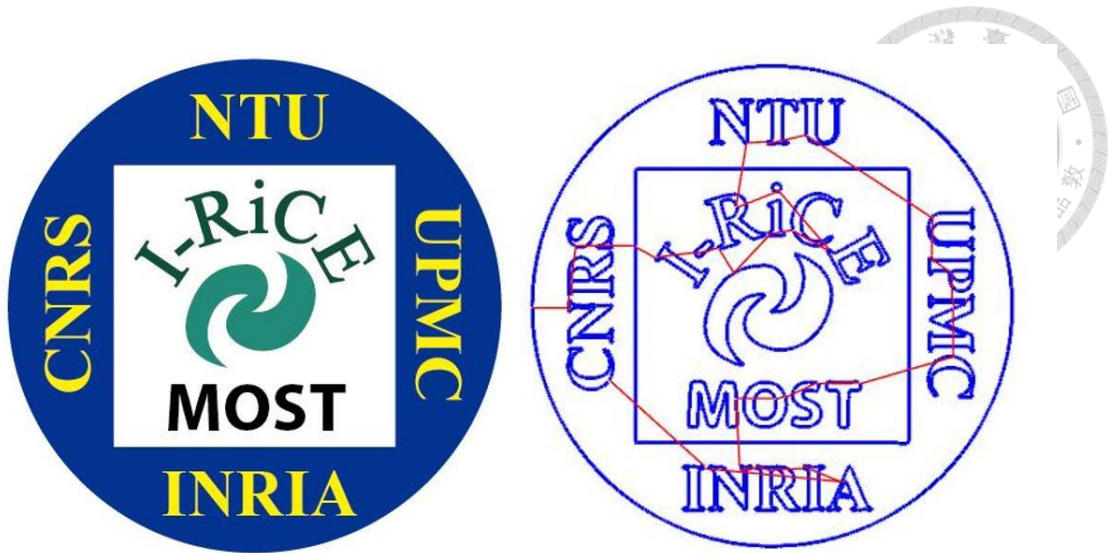
Figure 5.2-6 The left is 2D image and the right is the planned path by greedy algorithm. The red line is the transition path and the carving path is labeled as blue line.

The projection distortion evaluation, which is proposed in the paper [2], is a common used and quantitative analysis method. Compare the length between two adjacent points on 2D data with the distance between two corresponding points on 3D, the average error in length e_{l_ave} can be calculated by Equation (5-4).

$$e_{l\_ave} = \left(\sum_{i=1}^{N_p-1} |l_{2d\_i} - l_{3d\_i}| \right) / (N_p - 1) \qquad (5\text{-}4)$$

The N_p represents the number of the point on 2D path while l_{2d_i} and l_{3d_i} are the distance from the ith point to (i+1)th point on 2D and 3D individually. For example, Fig. 12 shows the two projection algorithms, and the red line is our proposed projection algorithm and the blue line is orthogonal projection method. In Table 15, the (a) and (c) can be flattened into the 2D plane without distortion. In other words, the edges, angles and areas of the triangles in the 3D mesh are transferred to 2D plane without any change. However, the (b) exists error when the surface of 3D mesh is flattened into 2D plane. As a result, the proposed algorithm can minimize error with the original surface to ensure
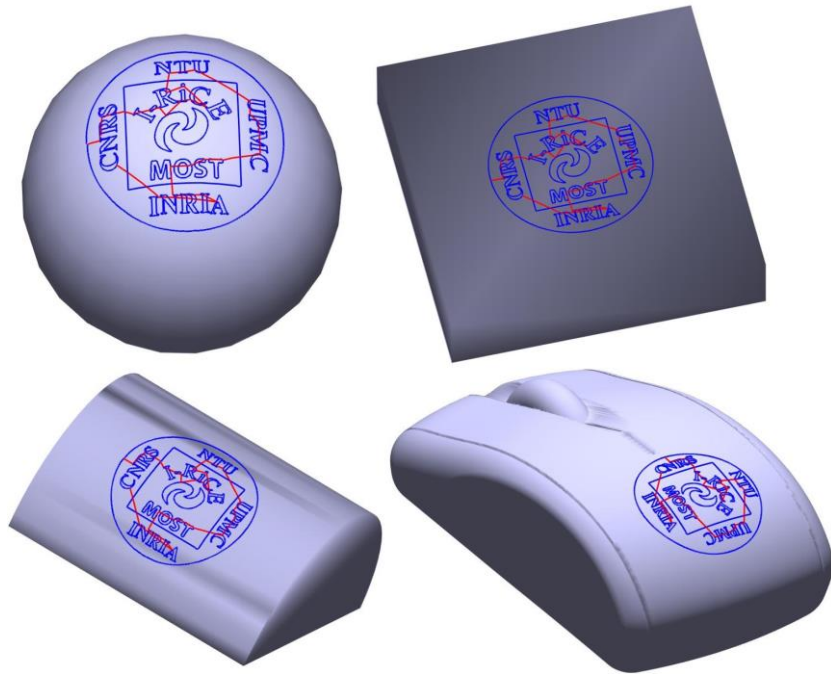
84

obtaining the better projection results.

Figure 5.2-7 Show the projected results on the geometric models.
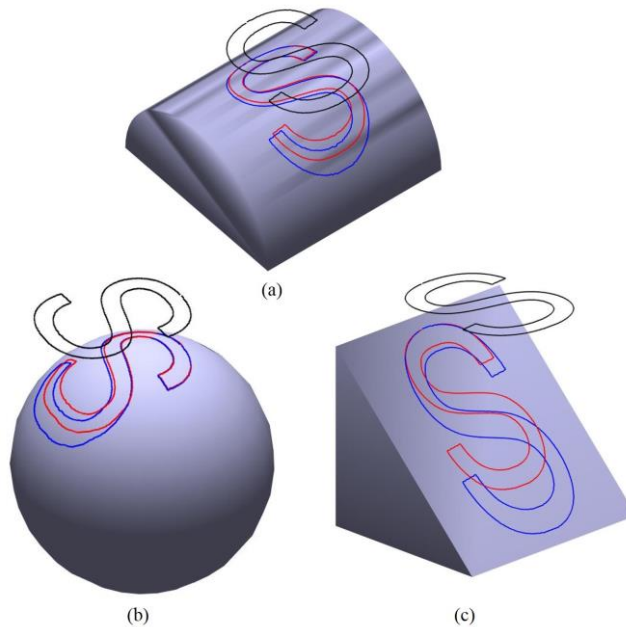

Figure 5.2-8 The black line which 2D data is projected onto the 3D different models. Compared with projection algorithms, the red line is our proposed algorithm and the blue line is orthogonal projection method.
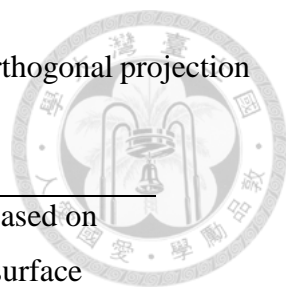
85

Table 15 Compare average length error (mm per unit) with orthogonal projection on projection results in Figure 5.2-8.

	Orthogonal projection	Projection based on flattening surface
(a)	0.0069	~0
(b)	0.0087	0.0013
(c)	0.025	~0

In this experiment, the additive and subtractive processing is shown in the Figure 5.2-9. Firstly, the 3D printer machine print the object by using the additive manufacturing, and then the subtractive tool is going to carve process after the additive manufacturing is completed.
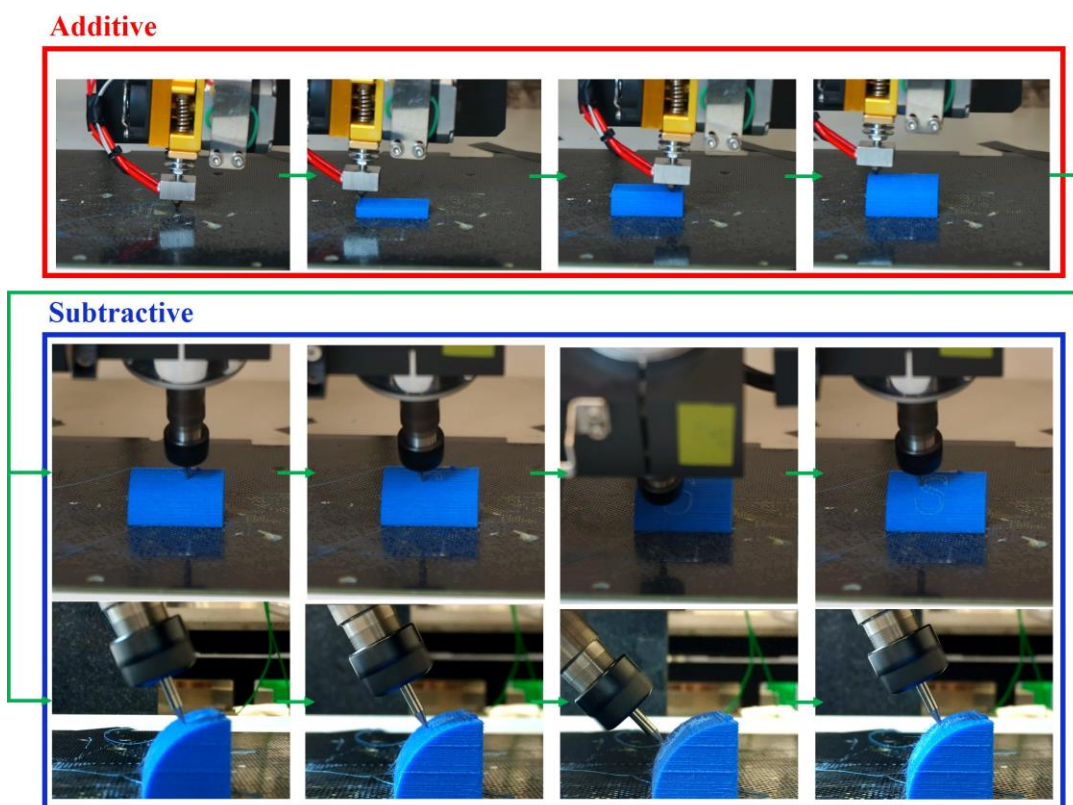
Figure 5.2-9 the process of additive and subtractive manufacturing with front view and side view

Figure 5.2-10 shows the carving result on the printed model. Using the above

86

projection procedure obtains the path for carving. Figure 5.2-10 (b) displays the blue and red curves on the 3D surface, and the carving path is labeled as blue line. Figure 5.2-10 (c) is the carving result on printed model.

(a)

(b)

(c)

Figure 5.2-10 (a) The original STL model. (b) The projected simulation on the model. (c) The carving result on printed model.

Chapter 6   Conclusions and future work

In this thesis, there are two parts about multiple heterogeneous objects fabrication and carving process. On the one hand, the proposed method i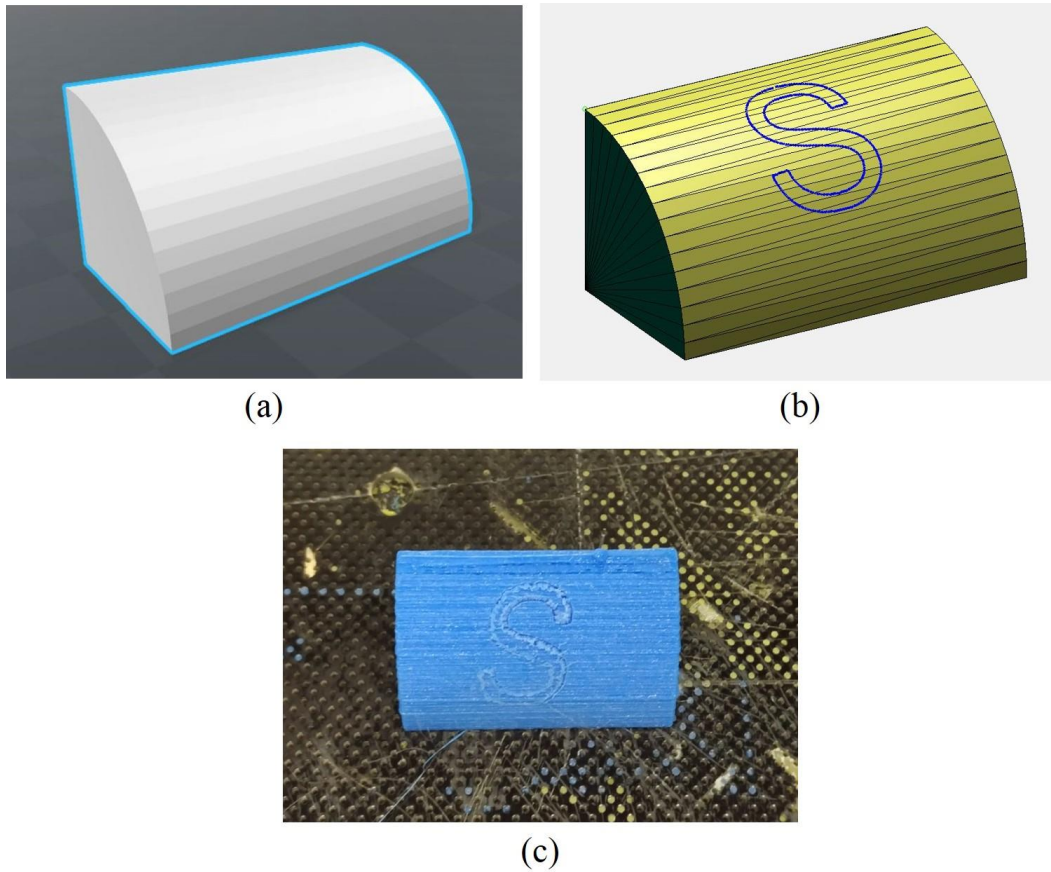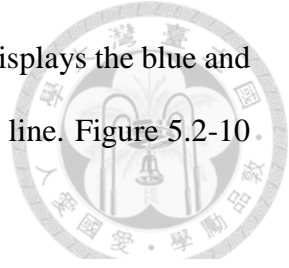s about optimizing the additive manufacturing path for multi-objects with generic algorithm. There are two important key to reduce the production time. One is motion path optimization and the other is that increase the speed of the extruder nozzle. In summary, proposed approach can significantly reduce the length of transition path comparing to the path which is produced by common slicing software to save extra production time.

On the other hand, an integrated gantry-type system combining additive and subtractive manufacturing is proposed to fabricate 3D models and then carve the designed shape on the surface of printed objects. In this paper, we proposed a new projection algorithm based on flattening surface to obtain the sculpturing path on the 3D surface. Therefore, the flattening surface process can combine the conformal mapping and spring mass model based on edge mesh which can minimize error with the original surface to ensure obtaining the better projection results. In addition, the hybrid process combining additive and subtractive processes completes the designed production. The additive process can print main structures of 3D model while the detailed part can be carved by subtractive process. The advantage of cooperation in this method is not only omits repositioning process but also preserves the accuracy of the production.

There are more applications for industrial manufacturing can be performed. In additive manufacturing, we plan to design the 5-DOF 3D printer machine to do more complex models. As for subtractive process, various other kinds of cutting tools like laser or water jet will also be used for corresponding materials.

88

Chapter 7   Other Applications

● Reverse engineering of machines

Reverse engineering, also known as back engineering, is the processes of extracting

knowledge or features from anything man-made and reconstructing it or reconstructing

anything based on the extracted information. In the experiment, using the Skanect 3D

scanning software [29] and Kinect one reconstructs the model and the printing result is
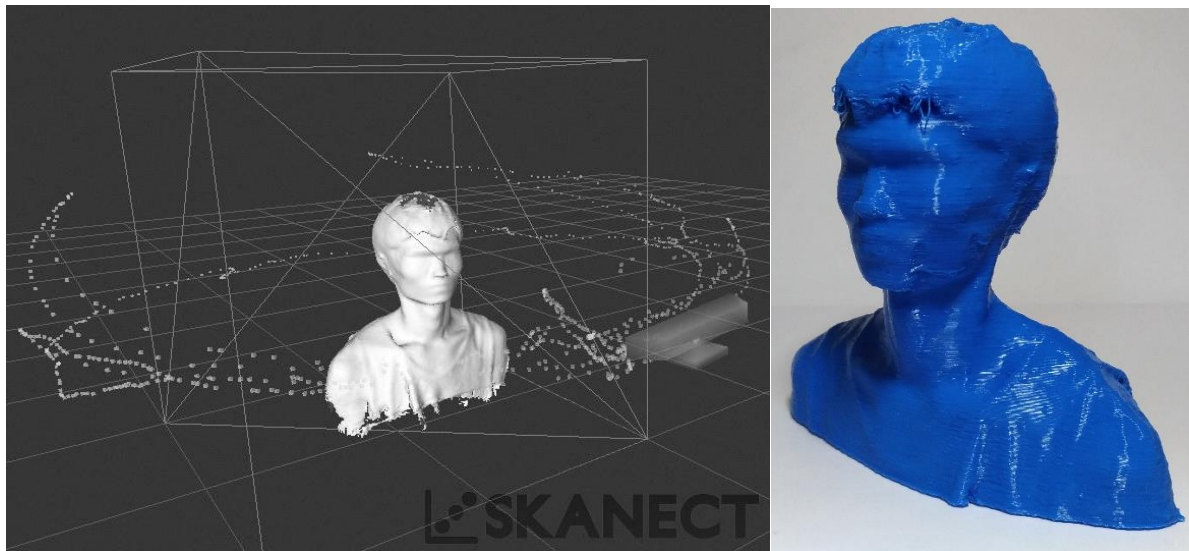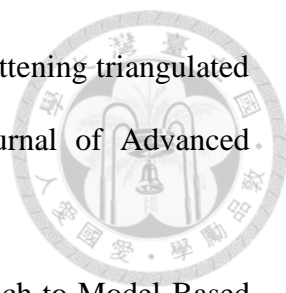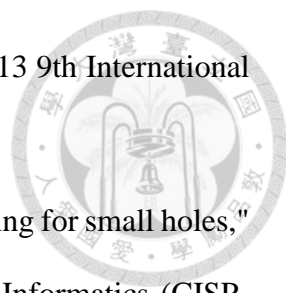
shown in Figure 7.1-1.

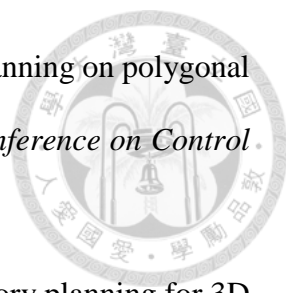Figure 7.1-2 Skanect 3D scanning software and printing result

References

[1] W. Du, Y. Tang, S. Leung, L. Tong, A. V. Vasilakos, and F. Qian, "Robust Order Scheduling in the Fashion Industry: A Multi-Objective Optimization Approach," *IEEE Transactions on Industrial Informatics*, 2017.

[2] B. Cao, J. Zhao, Z. Lv, and X. Liu, "A Distributed Parallel Cooperative Coevolutionary Multi-Objective Evolutionary Algorithm for Large-Scale Optimization," *IEEE Transactions on Industrial Informatics*, 2017.

[3] M. S. Brown and C. J. Pisula, "Conformal deskewing of non-planar documents," in *Computer Vision and Pattern Recognition, 2005. CVPR 2005. IEEE Computer Society Conference on*, 2005, vol. 1, pp. 998-1004: IEEE.

[4] Q. Li and J. Xue, "Conformal flattening of non-planar surface," in Advanced Computer Theory and Engineering (ICACTE), 2010 3rd International Conference on, 2010, vol. 1, pp. V1-676-V1-679: IEEE.

[5] A. Sheffer and E. de Sturler, "Parameterization of faceted surfaces for meshing using angle-based flattening," Engineering with computers, vol. 17, no. 3, pp. 326-337, 2001.

[6] A. Sheffer, B. Lévy, M. Mogilnitsky, and A. Bogomyakov, "ABF++: fast and robust angle based flattening," ACM Transactions on Graphics (TOG), vol. 24, no. 2, pp. 311-330, 2005.

[7] G. Chen, L.-s. Zhou, L.-l. An, and K. Zhang, "A novel surface flattening method based on mesh edges," in Intelligent System Design and Engineering Application (ISDEA), 2012 Second International Conference on, 2012, pp. 129-133: IEEE.

[8] J. Li, D. Zhang, G. Lu, Y. Peng, X. Wen, and Y. Sakaguti, "Flattening triangulated surfaces using a mass-spring model," The International Journal of Advanced Manufacturing Technology, vol. 25, no. 1, pp. 108-117, 2005.

[9] S. von Enzberg and A. Al-Hamadi, "A Multiresolution Approach to Model-Based 3-D Surface Quality Inspection," IEEE Transactions on Industrial Informatics, vol. 12, no. 4, pp. 1498-1507, 2016.

[10] F. Schmick, N. O. Lüders, and J. Wollnack, "Automated assembly of large CFRP structures: Adaptive filling of joining gaps with additive manufacturing," in Assembly and Manufacturing (ISAM), 2016 IEEE International Symposium on, 2016, pp. 126-132: IEEE.

[11] F. G. Sisca, C. M. Angioletti, M. Taisch, and J. A. Colwill, "Additive manufacturing as a strategic tool for industrial competition," in Research and Technologies for Society and Industry Leveraging a better tomorrow (RTSI), 2016 IEEE 2nd International Forum on, 2016, pp. 1-7: IEEE.

[12] S. Lin, C. Lin, D. Lin, and C. Chuang, "Laser additive manufacturing technology in titanium 64 implant of microstructure fabrication and analysis," in Nano/Micro Engineered and Molecular Systems (NEMS), 2013 8th IEEE International Conference on, 2013, pp. 594-597: IEEE.

[13] T. Wasley et al., "Enabling Rapid Production and Mass Customisation of Electronics Using Digitally Driven Hybrid Additive Manufacturing Techniques," in Electronic Components and Technology Conference (ECTC), 2016 IEEE 66th, 2016, pp. 849-856: IEEE.

[14] O. Arslan, B. Demirci, H. Altun, and N. S. Tunaboylu, "A novel rotation-invariant template matching based on HOG and AMDF for industrial laser cutting

applications," in Mechatronics and its Applications (ISMA), 2013 9th International Symposium on, 2013, pp. 1-5: IEEE.

[15] Z. Xia, K. Zhou, X. Li, and X. Cui, "A method of robot laser cutting for small holes," in Image and Signal Processing, BioMedical Engineering and Informatics (CISP-BMEI), International Congress on, 2016, pp. 1887-1891: IEEE.

[16] J. Giannatsis, A. Vassilakos, V. Canellidis, and V. Dedoussis, "Fabrication of graded structures by extrusion 3D Printing," in *Industrial Engineering and Engineering Management (IEEM), 2015 IEEE International Conference on*, 2015, pp. 175-179: IEEE.

[17] A. C. Brown and D. de Beer, "Development of a stereolithography (STL) slicing and G-code generation algorithm for an entry level 3-D printer," in *AFRICON, 2013*, 2013, pp. 1-5: IEEE.

[18] J.-J. Kim and J.-J. Lee, "Trajectory optimization with particle swarm optimization for manipulator motion planning," IEEE Transactions on Industrial Informatics, vol. 11, no. 3, pp. 620-631, 2015.

[19] M. Wojcik, L. Koszalka, I. Koszalka, and A. Kasprzak, "MZZ-GA Algorithm for Solving Path Optimization in 3D Printing," *Proceedings to 8th ICONS, IARIA*, vol. 30, pp. 30-35, 2015.

[20] S. Lensgraf and R. R. Mettu, "Beyond Layers: A 3D-Aware Toolpath Algorithm for Fused Filament Fabrication," in *2016 IEEE International Conference on Robotics and Automation (ICRA)*, 2016, pp. 3625 – 3631.

[21] K.-Y. Fok, N. Ganganath, C.-T. Cheng, and K. T. Chi, "A 3D printing path optimizer based on Christofides algorithm," in *Consumer Electronics-Taiwan (ICCE-TW), 2016 IEEE International Conference on*, 2016, pp. 1-2: IEEE.

[22] G. E. Jan, K. Fung, P.-Y. Wu, and S.-W. Leu, "Shortest path-planning on polygonal surfaces with O (nlog n) time," in *2016 IEEE International Conference on Control and Robotics Engineering (ICCRE)*, 2016, pp. 1-5: IEEE.

[23] N. Ganganath, C.-T. Cheng, K.-Y. Fok, and K. T. Chi, "Trajectory planning for 3D printing: a revisit to traveling salesman problem," in *Control, Automation and Robotics (ICCAR), 2016 2nd International Conference on*, 2016, pp. 287-290: IEEE.

[24] V. Roberge, M. Tarbouchi, and G. Labonté, "Comparison of parallel genetic algorithm and particle swarm optimization for real-time UAV path planning," IEEE Transactions on Industrial Informatics, vol. 9, no. 1, pp. 132-141, 2013.

[25] B. Thompson and H.-S. Yoon, "Efficient path planning algorithm for additive manufacturing systems," *IEEE Transactions on Components, Packaging and Manufacturing Technology*, vol. 4, no. 9, pp. 1555-1563, 2014.

[26] N. Volpato, R. Nakashima, L. Galvão, A. Barboza, P. Benevides, and L. Nunes, "Reducing repositioning distances in fused deposition-based processes using optimization algorithms," in *High Value Manufacturing: Advanced Research in Virtual and Rapid Prototyping: Proceedings of the 6th International Conference on Advanced Research in Virtual and Rapid Prototyping, Leiria, Portugal, 1-5 October*, 2013, 2013, p. 417: CRC Press.

[27] KISSlicer gcode generator is available at http://www.kisslicer.com/.

[28] Z. Zhu, V. Dhokia, and S. Newman, "A novel process planning approach for hybrid manufacturing consisting of additive, subtractive and inspection processes," in Industrial Engineering and Engineering Management (IEEM), 2012 IEEE International Conference on, 2012, pp. 1617-1621: IEEE.

[29] Skanect is available at http://skanect.occipital.com/download/

VITA

姓名：曾柏凱

性別：男

生日：11.01.1992

籍貫：台南市

學歷：

1. 民國 106 年　　國立臺灣大學電機工程學研究所

2. 民國 104 年　　國立臺灣科技大學電機工程學系畢業

3. 民國 100 年　　國立臺南高級工業職業學校電機科畢業

發表著作：

1. Ren C. Luo*, Po-Kai Tseng, "Trajectory Generation and Planning for Simultaneous 3D Printing of Multiple Objects," **published** by *the 26st IEEE International Symposium on Industrial Electronics (ISIE 2017),* 2017.

2. Ren C. Luo*, Po-Kai Tseng, "Carving 2D Image Onto 3D Curved Surface Using Hybrid Additive and Subtractive 3D Printing Process," **accepted** by *IEEE Advanced Robotics and Intelligent Systems (ARIS)*, 2017.

榮譽事績：

2016/09/01　第九屆上銀智慧機器手實作競賽　開發組　亞軍

疊疊樂　冠軍